Electronic Supplementary Information (ESI)

Beyond the TPP^+ "gold standard": A new generation mitochondrial delivery vector based on extended PN frameworks.

How Chee Ong,[a] João T. S. Coimbra,[b] Maria J. Ramos,[b] Bengang Xing,[a] Pedro A. Fernandes[b,*] and Felipe García[c,d*]

[a.] School of Physical and Mathematical Sciences, Division of Chemistry and Biological Chemistry, Nanyang Technological University, 21 Nanyang Link, 637371, Singapore

[b.] LAQV, REQUIMTE, Departamento de Química e Bioquímica, Faculdade de Ciências, Universidade do Porto, Rua do Campo Alegre s/n, 4169-007, Portugal.

[C] Departamento de Química Orgánica e Inorgánica, Facultad de Química, Universidad de Oviedo, Avda Julian Claveria 8, 33006, Asturias, Spain.

[d] School of Chemistry, Monash University, Clayton, Victoria 3800, Australia.

Content:

Experimental

1. Chemicals

Triphenylphosphine, hexachloroethane, bromine, methylamine, dimethylamine, disodium fluorescein and n-butyllithium were purchased from Sigma Aldrich, and all other chemicals (hexachloroethane and bromoethane) were purchased from TCI Chemicals. The starting materials were used without further purification. Solvents used were dried and stored under 4 Å molecular sieves. Reactions were carried out using standard Schlenk techniques and performed under argon. Human epithelial carcinoma cell line (HeLa) was purchased from ATCC ® (ATCC no. CCL-2).

2. Instrumentation

^{1}H, ^{13}C, $^{31}P\{^{1}H\}$ NMR spectra were collected using Bruker Avance III, 400 MHz and 500 MHz spectrometers with the ^{1}H, ^{13}C NMR chemical shifts internally referenced to the relevant residual solvent peaks. All NMR spectroscopic analysis were performed at room temperature (300 K). High-resolution mass spectra were obtained from Water Q-Tof Premier, with ESI mode. Reverse-phase HPLC analysis was performed on a Shimadzu Prominence-I LC-2030 using a C-8/C-18 analytical column at a flow rate of 1.0 mL/min for analysis. Resazurin Reduction Assays were measured by Tecan's Infinite M200 microplate reader. Confocal imaging was carried out on a Carl Zeiss LSM 800 confocal laser microscope.

3. Single crystal X-ray diffraction (SCXRD) studies

Diffraction-quality crystals were obtained by crystallization from acetonitrile/diethyl ether at room temperature. The crystals were mounted onto quartz fibers, and the X-ray diffraction intensity data were measured at 100 K with a Bruker Kappa diffractometer equipped with a CCD detector, employing Mo K_α radiation (λ = 0.71073 Å), with the SMART suite of programs.[1] All data were processed and corrected for Lorentz and polarization effects with SAINT and for absorption effects with SADABS.[2] Structural solution and refinement were carried out with the SHELXTL suite of programs.[3] The structures were solved by direct methods or Patterson maps to locate the heavy atoms, followed by difference maps for the light, non-hydrogen atoms. All non-hydrogen atoms were refined with anisotropic thermal parameters. CCDC 2084067/2084071/2084073/2084074 contains the supplementary crystallographic data for this paper. These data can be obtained free of charge from The Cambridge Crystallographic Data Centre via www.ccdc.cam.ac.uk/structures

4. Synthesis of delocalized lipophilic cations

The synthesis for compound **1, 5**, **6** and fluorescein methyl ester (methyl 2-(6-hydroxy-3-oxo-3H-xanthen-9-yl)benzoate) are achieved by following procedures in the literature [4-7] and hence they are not described here.

4.1. Synthesis of aminotriphenylphosphonium chloride

Triphenylphosphine (3.93 g, 15 mmol) and hexachloroethane (3.91 g, 16.5 mmol) was stirred in THF (30 mL) for 1 hour at room temperature. Ammonia gas was bubbled through the mixture for 20 minutes in an ice bath. The mixture was allowed to stir at room temperature for 2 hours and the solvent was removed in vacuo. The solids were extracted with 50 mL of water and 5 x 20 mL of chloroform. The combined organic layer was dried with magnesium sulfate and the product was recrystallized from chloroform/methanol/diethylether to obtain a white solid. (3.64 g, 70%)

^{1}H NMR (400 MHz, $CDCl_3$) δ 7.88 – 7.80 (m, 6H), 7.70 – 7.63 (m, 3H), 7.59 – 7.51 (m, 6H), 7.40 (s, 2H).

$^{31}P\{^{1}H\}$ NMR (162 MHz, $CDCl_3$) δ 35.66.

$^{13}C\{^{1}H\}$ NMR (101 MHz, $CDCl_3$) δ 134.08 (d, J = 3.1 Hz), 133.38 (d, J = 11.5 Hz), 129.48 (d, J = 13.4 Hz), 124.02 (d, J = 103.8 Hz).

TOF-MS-ES+ for $[M\text{-}Br]^+$: Calcd. m/z 278.1099; Found 278.1092.

4.2. Synthesis of compound 2

Triphenylphosphine (0.525g, 2 mmol) was dissolved in toluene (5 mL) and cooled in an ice bath. Bromine (0.319 g, 103 µL, 1 equiv) was added dropwise, and the solution was allowed to warm to room temperature. A mixture of methylamine solution (2 M in THF, 1 mL), triethylamine (0.202 g, 0.279 mL, 1 equiv) and toluene (4 mL) was added to the dibromotriphenylphosphorane solution and the mixture was stirred overnight at room temperature. The suspension was filtered, and the residue was washed with ice cold water and diethyl ether. The crude product was recrystallized in chloroform and ethyl acetate to obtain white crystals. (0.313 g, 42%)

^{1}H NMR (500 MHz, $CDCl_3$) δ 7.91 (s, 1H), 7.84 – 7.78 (m, 6H), 7.75 (td, J = 7.4, 1.6 Hz, 3H), 7.66 – 7.62 (m, 6H), 2.76 (dd, J = 13.8, 4.4 Hz, 3H).

^{31}P{^{1}H} NMR (202 MHz, $CDCl_3$) δ 38.93.

^{13}C{^{1}H} NMR (101 MHz, $CDCl_3$) δ 134.87 (d, J = 3.1 Hz), 133.57 (d, J = 11.0 Hz), 130.01 (d, J = 13.1 Hz), 121.17 (d, J = 102.9 Hz), 28.22 (d, J = 2.3 Hz).

Calcd. m/z 292.1255; Found 292.1255.

4.3. Synthesis of compound 3

Aminotriphenylphosphonium chloride (0.313 g, 1 mmol) was suspended in THF (8 mL) in an ice-bath, and n-butyllithium (2 M in cyclohexane, 1.5 mL, 3 mmol) was added into the mixture. After the solids dissolved, the mixture was stirred for an additional 10 minutes. Diphenylchlorophosphine (0.353 g, 0.296 mL, 1.6 mmol) was added, and the mixture was warmed to room temperature and allowed to stir for an additional 30 minutes. Bromoethane (1.09 g, 0.741 mL, 10 mmol) was added, and the mixture was allowed to stir overnight. The mixture was quenched with ethanol, and the solvent was removed in vacuo. The crude mixture was extracted with 20 mL of water and 3 x 10 mL of dichloromethane. The organic layer was concentrated, and the product was precipitated with diethylether. The solids were recrystallized in dichloromethane and diethylether to obtain white solids. (0.552 g, 96 %).

^{1}H NMR (400 MHz, $CDCl_3$) δ 7.73 – 7.41 (m, 25H), 2.65 (dq, J = 10.7, 7.5 Hz, 2H), 1.10 (dt, J = 19.7, 7.5 Hz, 3H).

$^{31}P\{^{1}H\}$ NMR (162 MHz, $CDCl_3$) δ 29.02 (d, J = 5.2 Hz), 19.76 (d, J = 5.1 Hz).

$^{13}C\{^{1}H\}$ NMR (101 MHz, $CDCl_3$) δ 133.86 (d, J = 3.1 Hz), 133.52 (d, J = 3.0 Hz), 132.06 (d, J = 11.2 Hz), 131.44 (d, J = 10.8 Hz), 129.69 (d, J = 13.1 Hz), 129.60 (d, J = 12.7 Hz), 127.33 (dd, J = 107.0, 1.9 Hz), 126.91 (dd, J = 102.0, 3.4 Hz), 22.51 (d, J = 70.7 Hz), 6.11 (d, J = 5.2 Hz).

TOF-MS-ES+ for [M-Br]+ : Calcd. m/z 490.1853; Found 490.1853.

4.4. Synthesis of compound 4

Dimethylamine (2 M in THF, 1 mL, 2 mmol) was added to a biphasic mixture of aqueous sodium hydroxide (2 M, 5 mL)/toluene (5 mL) and the mixture was cooled in an ice bath. Bromine (0.319 g, 103 µL, 2 mmol) was added, and the mixture was stirred for an additional 30 minutes. The organic layer was separated and the aqueous layer was extracted with 2 mL of toluene. The combined organic phase was washed with brine and dried in $MgSO_4$. Triphenylphosphine (0.262 g, 1 mmol) was dissolved in 2 mL of toluene, and the bromamine solution was added dropwise in an ice bath. The solution was extracted with water and the water was removed by boiling. The crude product was purified via flash column chromatography and the product was recrystallized in chloroform/diethylether to obtain white crystals. (0.071 g, 18 %)

^{1}H NMR (400 MHz, $CDCl_3$) δ 7.92 – 7.81 (m, 9H), 7.81 – 7.72 (m, 6H), 3.08 (d, J = 10.5 Hz, 6H).

$^{31}P\{^{1}H\}$ NMR (162 MHz, $CDCl_3$) δ 46.44.

$^{13}C\{^{1}H\}$ NMR (101 MHz, $CDCl_3$) δ 135.65 (d, J = 2.9 Hz), 133.98 (d, J = 10.7 Hz), 130.66 (d, J = 13.0 Hz), 119.69 (d, J = 102.6 Hz), 39.68 (d, J = 3.3 Hz).

Calcd. m/z 306.1412; Found 306.1408.

4.5. Synthesis of compound 7

Aminotriphenylphosphonium chloride (0.628 g, 2 mmol) was suspended in THF (10 mL) in an ice-bath, and n-butyllithium (2 M in cyclohexane, 2.2 mL, 4.4 mmol) was added into the mixture. After the solids dissolved, the mixture was stirred for an additional 15 minutes. Diphenylchlorophosphine (0.441 g, 0.359 mL, 2 mmol) was added, and the mixture was warmed to room temperature and allowed to stir for an additional 15 minutes. 1,5-dibromopentane (4.60 g, 2.72 mL, 20 mmol) was added, and the mixture was allowed to stir overnight. The solvent was removed in vacuo and the crude product was purified by flash column chromatography (dichloromethane/MeOH) to obtain a white waxy solid. (0.874 g, 63 %)

Fluorescein methyl ester (0.876 g, 2.53 mmol, 2 equiv) and potassium carbonate (0.524 g, 3.79 mmol, 3 equiv) and dimethylformamide (10 mL) was added to the solids obtained, and the suspension was heated at 90°C for 2 hours. The mixture was allowed to cool to room temperature and chloroform (50 mL) was added and the organic phase was washed with 3 x 50 mL of water. The organic layer was dried using sodium sulfate, and the solvents were removed in vacuo. The crude product was purified by flash column chromatography (100:10:1 dichloromethane:MeOH:trifluoroacetic acid). The product was redissolved in chloroform (10 mL) and washed with 5 x 10 mL of 1 M sodium carbonate and washed with aqueous sodium bromide (2 M, 50 mL). The organic layer was dried in sodium sulfate and the solvent was removed in vacuo to obtain an orange powder. (0.306 g, 25%)

^{1}H NMR (400 MHz, $CDCl_3$) δ 8.26 (d, J = 7.6 Hz, 1H), 7.81 – 7.44 (m, 27H), 7.32 (d, J = 7.7 Hz, 1H), 6.87 (dd, J = 9.3, 6.4 Hz, 2H), 6.79 (d, J = 2.4 Hz, 1H), 6.72 (dd, J = 8.9, 2.5 Hz, 1H), 6.55 (dd, J = 9.7, 1.9 Hz, 1H), 6.46 (d, J = 1.9 Hz, 1H), 3.98 (t, J = 6.2 Hz, 2H), 3.65 (s, 3H), 2.97 – 2.75 (m, 2H), 1.79 – 1.69 (m, 2H), 1.61 – 1.46 (m, 4H).

^{31}P{^{1}H} NMR (162 MHz, $CDCl_3$) δ 27.48 (d, J = 5.2 Hz), 19.75 (d, J = 6.0 Hz).

TOF-MS-ES+ for [M-Br]+ : Calcd. m/z 876.3008; Found 876.3005.

5. Measurement of lipophilicity

Lipophilicity was determined by measuring octanol−water partition coefficient using HPLC measurements as described in the literature.[8] Calibration curves were obtained from standard solutions prepared (20 – 100 µM). A 100 µM sample of phosphonium salt in octanol-saturated water was stirred vigorously with water-saturated octanol in a 1.5 mL microtube and allowed to sit for 10 minutes. The two phases were separated by centrifugation, and the concentration of the phosphonium salt in the aqueous layer was quantified by HPLC using a UV detector (220 nm). The peak area in the water layer was used to calculate the partition coefficient (log P):

$$\log P = log\left[\left(\frac{A_{std}}{A_w} - 1\right)\left(\frac{V_w}{V_o}\right)\right]$$

where A_{std} and A_w represents the peak area for a 100 µM standard and the aqueous layer, respectively. V_w and V_o represents the volume of water and octanol used in the mixture. The measurement for each compound was repeated 3 times and the results and solvent ratios used are shown below in **Table S1**.

Table S1. Results for lipophilicity measurements

Compound	*log P (octanol/water)*	*St. Dev.*	*log P (octanol/PBS)*	*St. Dev.*
1	-1.363	0.092	-0.429	0.005
2	-1.277	0.005	0.527	0.214
3	0.507	0.0324	-	-
6	0.417	0.040	-	-
7	2.549	0.098	-	-

6. Cells culture and determination of the half maximal inhibitory concentration (IC_{50}) test

HeLa cells were cultured in Dulbecco's modified Eagle's medium (DMEM) solution with 10% fetal bovine serum (FBS) and 1% Penicillin/Streptomycin under humidified atmosphere of 5% CO_2 at 37 °C. Resazurin sodium salt was dissolved in PBS (0.2 mg/mL) to make a stock solution, which was diluted in DMEM w/o phenol red to 0.02 mg/mL before use. Stock solutions (10 µM) were prepared by dissolving the salts in DMSO. The HeLa cells were seeded on a 96-wells containing 10000 cells per well in 100 µL DMEM media and incubated overnight before the addition of stock solutions containing TPP^+ salts. Upon incubation at 37 °C for an additional 72 h, the media was removed, and the cells were washed with PBS. Resazurin solution (100µL) was added to each well before incubation for 2 h at 37 °C. The samples were excited using a 560 nm light and the fluorescence was recorded on a Tecan's Infinite M200 microplate reader using a 590 nm emission filter. Different concentrations of were used and for each concentration and was performed in triplicate. The experiment was repeated three times and the IC_{50} was determined from the plot of viability against concentration of samples.

7. Confocal microscopy

HeLa cells were cultured in Dulbecco's modified Eagle's medium (DMEM) solution with 10% fetal bovine serum (FBS) and 1% Penicillin/Streptomycin under humidified atmosphere of 5% CO_2 at 37 °C. 25 x 10^4 HeLa cells were seeded on a microscope slide (Ibidi #80827) overnight in 200 µL of DMEM, and was subsequently treated with compounds 6 or 7. (100 nM, λ_{ex} = 488 nm) and Mitotracker DeepRed FM (50 nM, λ_{ex} = 640 nm) at 37 °C for 1 hour. The cells were washed 3 x 200 µL of PBS, and the chambers were filled with DMEM for imaging.

8. Computational methods

8.1. Molecular dynamics simulations

Molecular dynamics (MD) simulations of the studied compounds were performed with the GROMACS 2018 software.[9-11]

System modeling. Our all-atom hydrated bilayer model system was composed of 72 1-palmitoyl-2-oleoyl-glycero-3-phosphocholine (POPC) lipids (36 lipids per leaflet), a hydration level of 60 water molecules per lipid, and an ionic concentration of *ca.* 0.15 M NaCl. It was assembled using the CHARMM-GUI interface using the AMBER force field.[12-15] After an initial minimization and equilibration of the system, we have inserted two replicas of the studied compounds at different bilayer depths in the simulation box: one of the replicas was inserted in the water phase, and the other at the center of the lipid bilayer (see next sections for details).

The cations were parameterized with the Antechamber program,[16] following a standard protocol: i) molecular mechanics parameters for bonded and van der Waals terms were extracted from the second-generation general amber force field (GAFF2); and ii) restrained electrostatic potential (RESP) charges[17] were derived at the HF/6-31G(d)//B3LYP/6-31G(d) level of theory. The conversion from amber-generated files to GROMACS-compatible ones was achieved with parmed.[18] We have confirmed that our optimized structures were true stationary points by performing a frequency calculation. All quantum mechanics calculations were performed with the Gaussian 09 software.[19]

Molecular dynamics simulations parameters. The all-atom simulations were performed with the GROMACS 2018 software, with the Verlet cut-off scheme. A non-bonded cut-off value of 1.0 nm was employed. The LINCS constraint algorithm was applied to all bonds involving hydrogen atoms, and for the production stage to all bonds. We have also employed a hydrogen mass repartition protocol for the production stage,[20] which allowed for an integration time step of 4 fs. Temperature was set to 298.15 K with the v-rescale thermostat (0.5 ps time constant for coupling for the production stage and 1 ps for the equilibration stages),[21] and a semi-isotropic pressure scaling to 1 atm was maintained with the Parrinello–Rahman barostat (5 ps time constant for coupling). During the NPT equilibration, the Berendsen barostat was employed. Dispersion corrections were applied to energy and pressure terms. Periodic boundary conditions were considered, and long-range electrostatic interactions were treated by a Particle Mesh Ewald (PME) scheme. The center of mass motion was removed in a linear fashion and individually for the upper and lower leaflets and the rest of the system (including the solvent, ions and the two solute molecules).

Umbrella sampling simulations and analysis. The hydrated bilayers coming from CHARMM-GUI were minimized and equilibrated in the NVT and NPT ensembles. Subsequently, an NPT conventional MD simulation of 300 ns was run. From the density profiles and as in previous works,[22-24] we have defined a four-region model to aid in the analysis of the PMFs. Region I contained only the hydrophobic lipid tails. Region II contained both hydrophobic tails and the initial portion of the polar headgroup density, ending where the lipid tail density intercepted the choline density. Region III

contained most of the charged phosphate and choline density. Finally, region IV was composed primarily of bulk water, and a small portion of the lipid's headgroup density.

Two replicas of each compound were inserted at different bilayer depths using the last structure of the previous run – one in the water phase and the other near the bilayer's center. The interactions with the hydrated bilayer system were then gradually switched on during 7.5 ns, with the compounds harmonically restrained to the initial positions relative to the bilayer's COM (with a harmonic force constant of 2000 kJ·mol^{-1}·nm^{-2}). Afterwards, a constant pulling simulation of 50 ns was performed to sample the desired translocation coordinate (pulling rate of -0.000074 nm·ps^{-1}). The translocation coordinate in this case was defined by the COM distance between the solute and the lipid bilayer and was discretized into 38 sampling windows spaced by 0.1 nm. This comprised the COM distances of [-3.5; 0.2] nm and [-0.2; 3.5] nm, depending on whether the compound started in the water phase or near the center of the bilayer. Then production runs were performed for 160 ns (with a harmonic force constant of 1500 kJ·mol^{-1}·nm^{-2}). The binding free energy, ΔG°_{bind}, was then derived from the energy profile using equation [1]:[25-26]

$$\Delta G^{\circ}_{bind} = -k_B T ln\left(\frac{1}{2z_b}\int_{-z_b}^{z_b} e^{-\beta w(z)} dz\right) \quad \textbf{[1]}$$

where $z_b = 3.4\ nm$ represents the distance at which the potential of mean force (PMF), $w(z)$, is zero and $\beta = 1/k_B T$, where *T* is adjusted to the temperature in which the profiles were generated, and k_B represents the Boltzmann constant. The partition coefficient, *P* can then be derived using equation [2]:[27]

$$P = e^{-\beta \Delta G^{\circ}_{bind}} \quad [2]$$

For the calculation of the binding free energies, we have considered the energy profiles produced from the last 100 ns of each window of the production runs. These were assessed with the weighted histogram analysis method (WHAM) tool[28] available in GROMACS 2018. A bootstrapping analysis (200 bootstraps) was also performed to assess for the error of the energy profile.

In **Figure S1**, we present the translocation free energy profile of all five cations (**1** – **5**) in a POPC hydrated bilayer system.

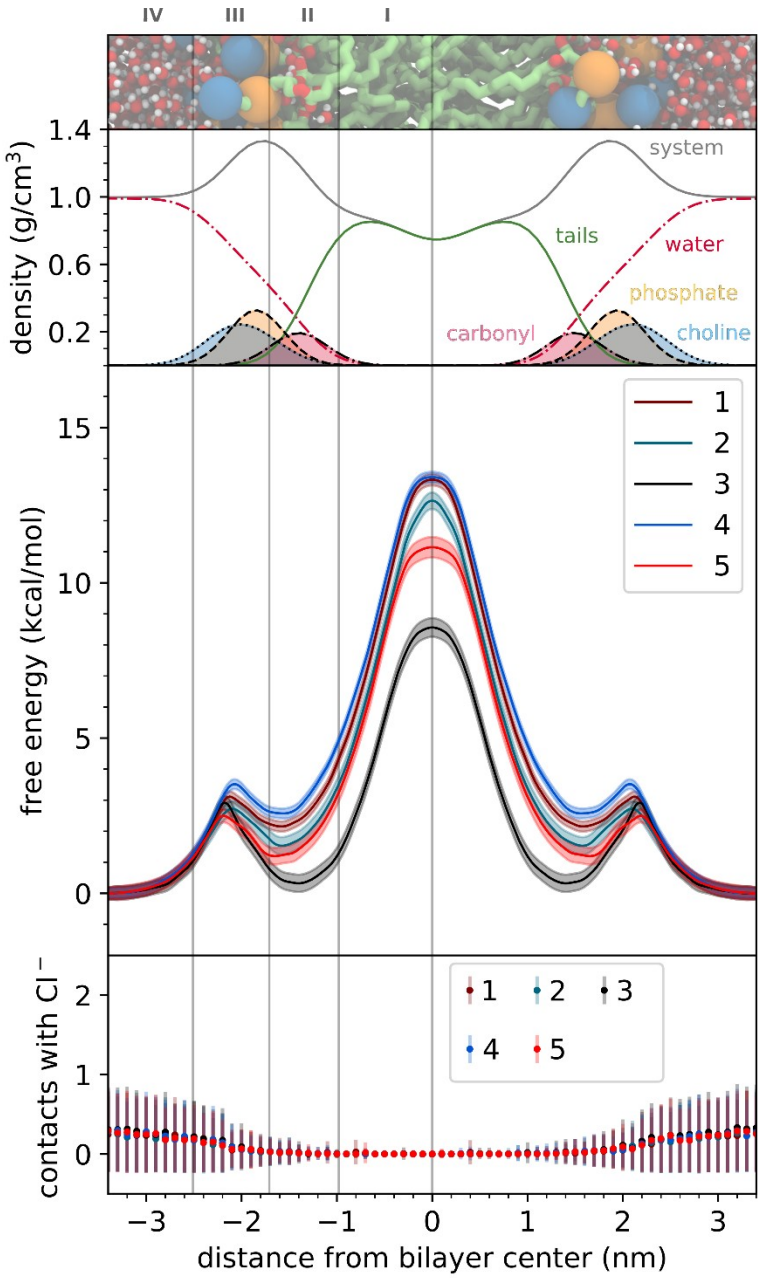

Figure S1. (Top 2 panels) Hydrated bilayer system and the partial density profiles for the different functional groups or molecules in the system. (Third panel) Free energy profiles for the translocation of selected cations **1** – **5**. (Bottom panel) Average number of contacts of any of the studied cations with Cl- counter-ions in the simulation cell (considering a distance threshold of 0.6 nm). Membrane regions (from left to right): region IV (bulk water); region III (charged phosphate and choline groups); region II (hydrophobic tails and a portion of the polar headgroup); and region I (hydrophobic lipid tails).

In **Table S2**, we provide additional parameters of the free energy diagrams for the cations' translocation through the hydrated bilayer system. A depiction of these parameters is also presented in **Figure S2.**

Table S2. Additional parameters of the energy profile diagrams**.** We show the maximum at region III, ΔG_{max}; the minimum of the profile after the membrane entry and located in region II, ΔG_{min}; and the barrier at the centre of the bilayer that is in region I, ΔG_B. ΔG_B was determined from the difference between maximum and minimum values of the energy profiles.

compound	ΔG_{max}/ kcal·mol^{-1}	ΔG_{min} / kcal·mol^{-1} [a]	ΔG_B / kcal·mol^{-1}
1	3.17	2.14	13.33
2	2.76	1.52	12.66
3	3.00	0.31	8.58
4	3.55	2.56	13.41
5	2.54	1.18	11.16

[a] The free energy profiles in region II did not drop below zero, but we have presented the value of the energy profile at the first minimum after the membrane entry.

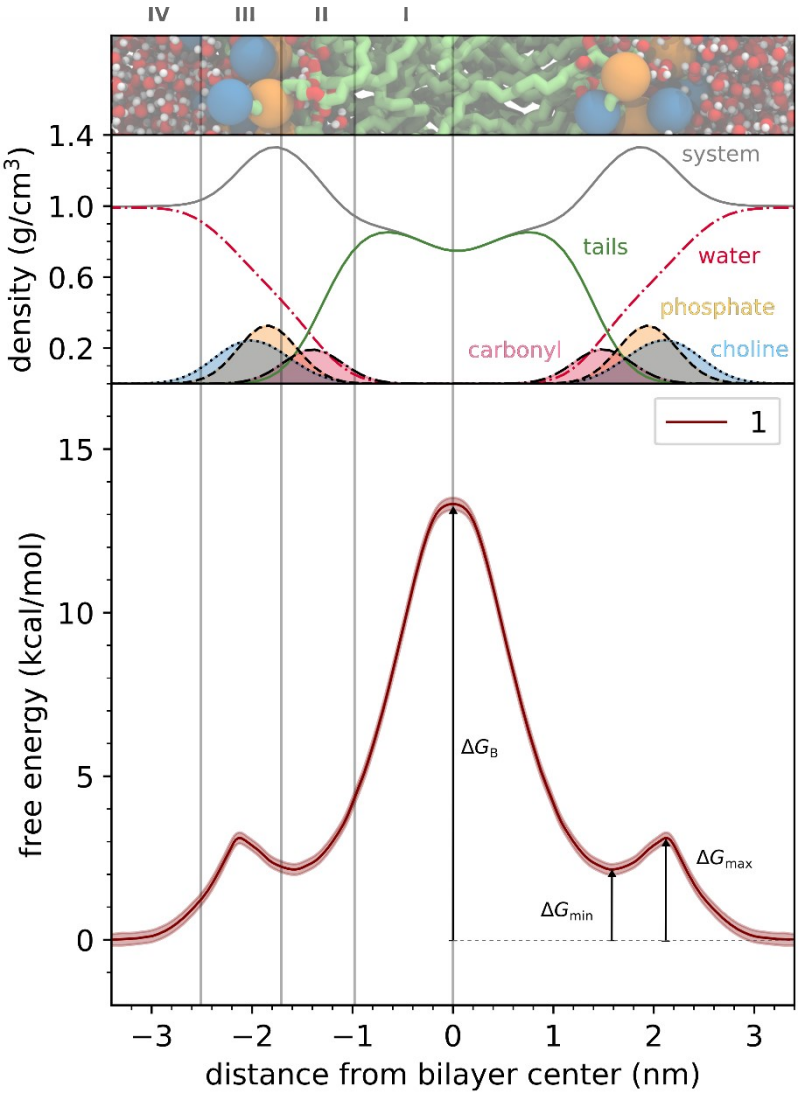

Figure S2. (Top 2 panels) Hydrated bilayer model system and the partial density profiles for the different functional groups or molecules in the system. Membrane regions (from left to right): region IV (bulk water); region III (charged phosphate and choline groups); region II (hydrophobic tails and a portion of the polar headgroup); and region I (hydrophobic lipid tails). (Bottom panel) Free energy profiles for the translocation of cation **1** and illustration of ΔG_{min}, ΔG_{max} and ΔG_B.

Visual inspection of the simulations was attained with the VMD 1.9.3 software.[30]

9.1. Quantum mechanics calculations

All calculations have been performed with the Gaussian 09 software. The evaluated parameters included the isotropic polarizability (α), dipole moment (μ), and frontier molecular orbitals (E_{HOMO}, $E_{HOMO-LUMO}$). These have been determined at the ωB97XD/6-311++G(d,p) level of theory, after a geometry optimization and frequency calculation at the same level. The results are presented in Table S3. In these calculations we have used the default optimization parameters of Gaussian 09.

Table S3. Polarizabilities, dipole moment and frontier molecular orbitals (E_{HOMO}, $E_{HOMO-LUMO}$) of cations **1** – **5**, determined at the ωB97XD/6-311++G(d,p) level of theory.

Compound	Polarizability / Bohr^3	Dipole moment / Debye	HOMO / eV	$E_{HOMO-LUMO}$ / eV
1	239.23	0.923	-12.530	9.680
2	235.04	1.316	-12.482	9.495
3	396.38	1.784	-11.770	9.510
4	246.80	0.928	-12.405	9.414
5	250.40	0.709	-12.372	9.362

Electrostatic surface potentials (ESP) have been obtained as well, and the MultiWfn program (version 3.3.9)[31] was used to determine the maximum of the electrostatic potential on the molecular surface, $V_{S,max}$. A representation of the ESP and $V_{S,max}$ for each of the cations was rendered with the VMD program.

The correlation of $V_{S,max}$ and $logP_{mem}$ with IC_{50} results is shown in **Figure S3**.

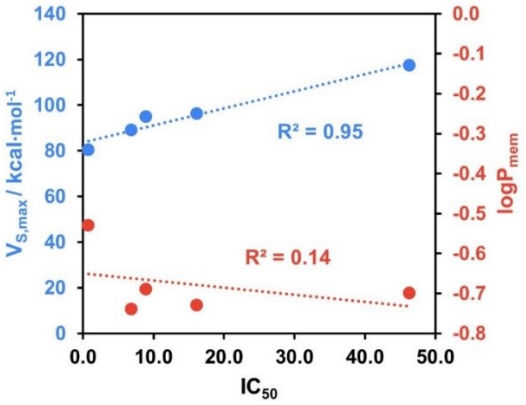

Figure S3. Linear correlation between $V_{S,max}$ and $logP_{mem}$ against IC_{50} experimental results for cations **1** – **5**.

The $V_{s,max}$ of additional compounds (previously studied by our group) was also determined. The additional compounds are represented in **Figure S4**, together with the IC_{50} and logP experimental results gathered from the literature in **Table S4**.

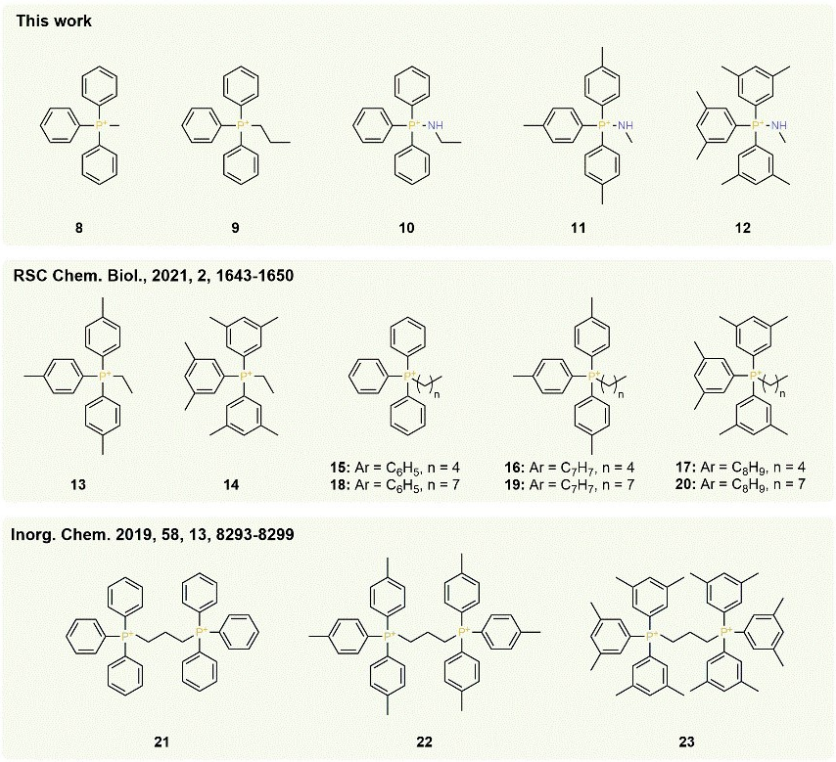

Figure S4. Additional mitochondrial vectors evaluated in this study.

Table S4. Experimental data for compounds **8 – 23.**

Compound	IC_{50} (± 95% CI) / µM	logP (± SD)	$V_{s,max}$ (kcal·mol^{-1})
8	24.78 ± 2.41	-1.50 ± 0.01	97.93
9	5.45 ± 1.30	-	94.27
10	33.63 ± 4.35	-	108.86
11	1.87 ± 0.38	-0.27 ± 0.04	106.44
12	1.32 ± 0.27	0.43 ± 0.01	104.67
13	3.83 ± 0.50	-0.50 ± 0.05	91.75
14	0.80 ± 0.06	0.08 ± 0.02	88.71
15	1.64 ± 0.14	-0.84 ± 0.01	93.34
16	0.45 ± 0.05	0.26 ± 0.02	90.12
17	0.36 ± 0.04	0.90 ± 0.01	87.96
18	0.34 ± 0.03	0.22 ± 0.02	92.72
19	0.30 ± 0.04	1.57 ± 0.02	89.80
20	0.32 ± 0.06	2.25 ± 0.05	87.68
21	181.26 ± 7.58	-1.62 ± 0.13	148.88
22	21.25 ± 1.59	-0.12 ± 0.03	139.50
23	5.56 ± 0.26	0.70 ± 0.08	136.49

Different correlations of $V_{S,max}$ with IC_{50} results are shown in **Figure S5**.

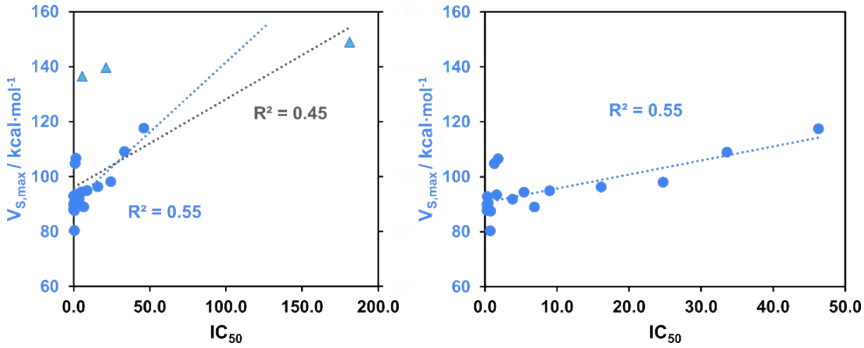

Figure S5. Linear correlation between $V_{S,max}$ against IC_{50} experimental results for cations **1** – **5**, **8** – **23** (left) and **1** – **5**, **8** – **20** (right).

Natural atomic charges derived from a NBO analysis of cations **1** and **2** ion-pairs (with Cl^-) have been determined at the ωB97XD/6-311++G(d,p)//ωB97XD/6-31G(d,p) and SMD(n-Hexane)-ωB97XD/6-311++G(d,p)// SMD(n-Hexane)-ωB97XD/6-31G(d,p) levels of theory. The charge of Cl^- while in a complex with cations **1** and **2** (in gas-phase and n-hexane), is represented in **Figure S6**.

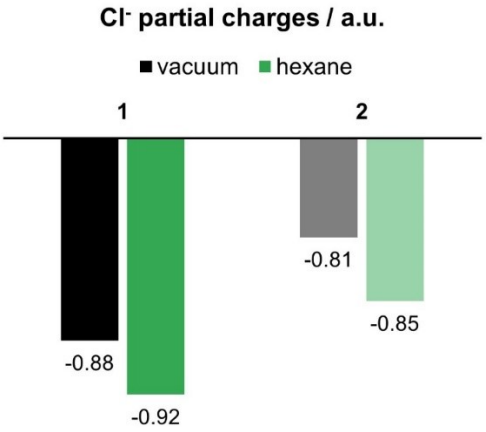

Figure S6. Partial charges on each Cl^- in the DLC:anion complexes of **1** and **2**.

Relevant free energies for the comparison of free-cation and ion-pair transfer of the cations from water to hexane are highlighted in bold in **Table S5**. These comprehend the free energy of transfer between water and n-Hexane and in the case of the ion-pairs the ion-pairing free energies in water. These calculations revealed that cation **1** and **2** show similar transfer free energies, but **2** seems to be more favourably transported as an ion-pair, whereas for **1**, the ion-pair increases the penalty for transferring from water to n-hexane.

Table S5. Free energies for the transfer of ions and ion-pairs from water (aq) to hexane (hex) – $\Delta_t G^*$(S, aq → hex), and for ion-pair formation in water – $\Delta_{ip} G^*$(aq). These were determined at the (SMD)-ωB97XD/6-311++G(d,p)//(SMD)-ωB97XD/6-31G(d,p) level of theory. Energies are expressed in kJ/mol and distances in Å.

Compound	$\Delta_t G^*$(S, aq → hex)	$\Delta_{ip} G^*$(aq)	$\Delta_t G^*$(S, aq → hex) + $\Delta_{ip} G^*$(aq)	Ion-pair distances (aq/hex)
1	**49**	-	-	-
2	**49**	-	-	-
1·Cl⁻	50	14	**64**	**2.53/2.33**
2·Cl⁻	35	3	**38**	**2.11/1.97**

The protocol summarizes as follows. All calculations were performed with the Gaussian 09 software. Final free energy values have been determined at the ωB97XD/6-311++G(d,p)//ωB97XD/6-31G(d,p) and SMD(solvent)-ωB97XD/6-311++G(d,p)// SMD(solvent)-ωB97XD/6-31G(d,p) levels of theory. We have employed a tight optimization criterion and an ultrafine grid in all optimizations. The SMD solvation model was used with the default Gaussian 09 values for water and n-hexane solvents. Default solvation radii were used, except for Cl^-, whose solvation radius was reduced to 1.8 Å in order

to better reproduce the experimental free energy of hydration of Cl^-.[32] The thermal contributions to the free energy were also determined. Grimme's quasi-RRHO approach was used to calculate free energies at 298.15 K, to avoid large entropy contributions from very low vibrational modes. We used a cut-off of 150 cm^{-1}.

We express all thermodynamic quantities in solution with reference to a fixed-solute equal-concentrations standard state, indicated by *, with a concentration of $c^* = 1\ mol \cdot L^{-1}$. For ion-pairing free energies, the free energy change therefore includes a correction of 7.9 $kJ \cdot mol^{-1}$.

9. NMR Spectra

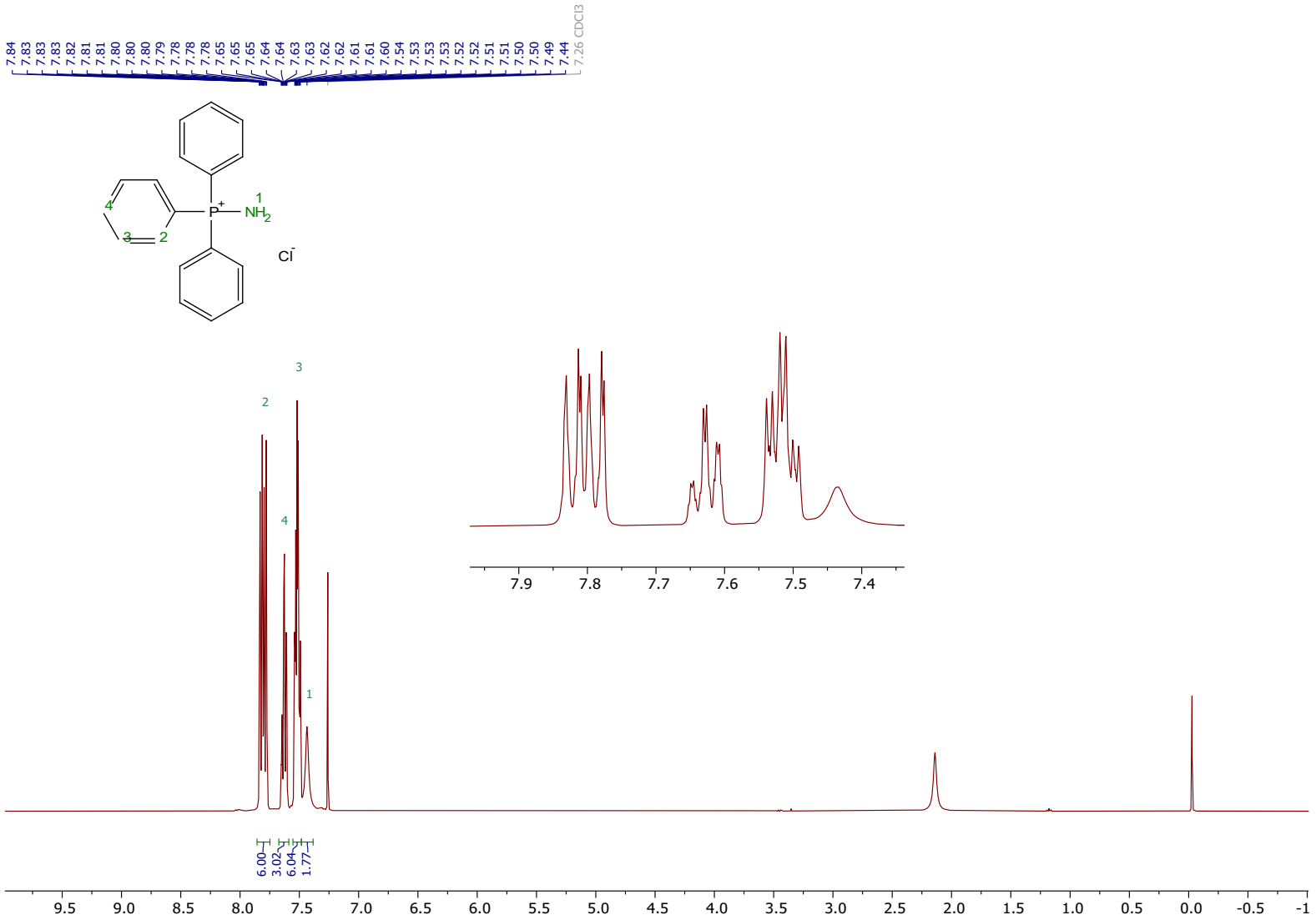

Figure S7. ^{1}H NMR spectrum of aminotriphenylphosphonium chloride

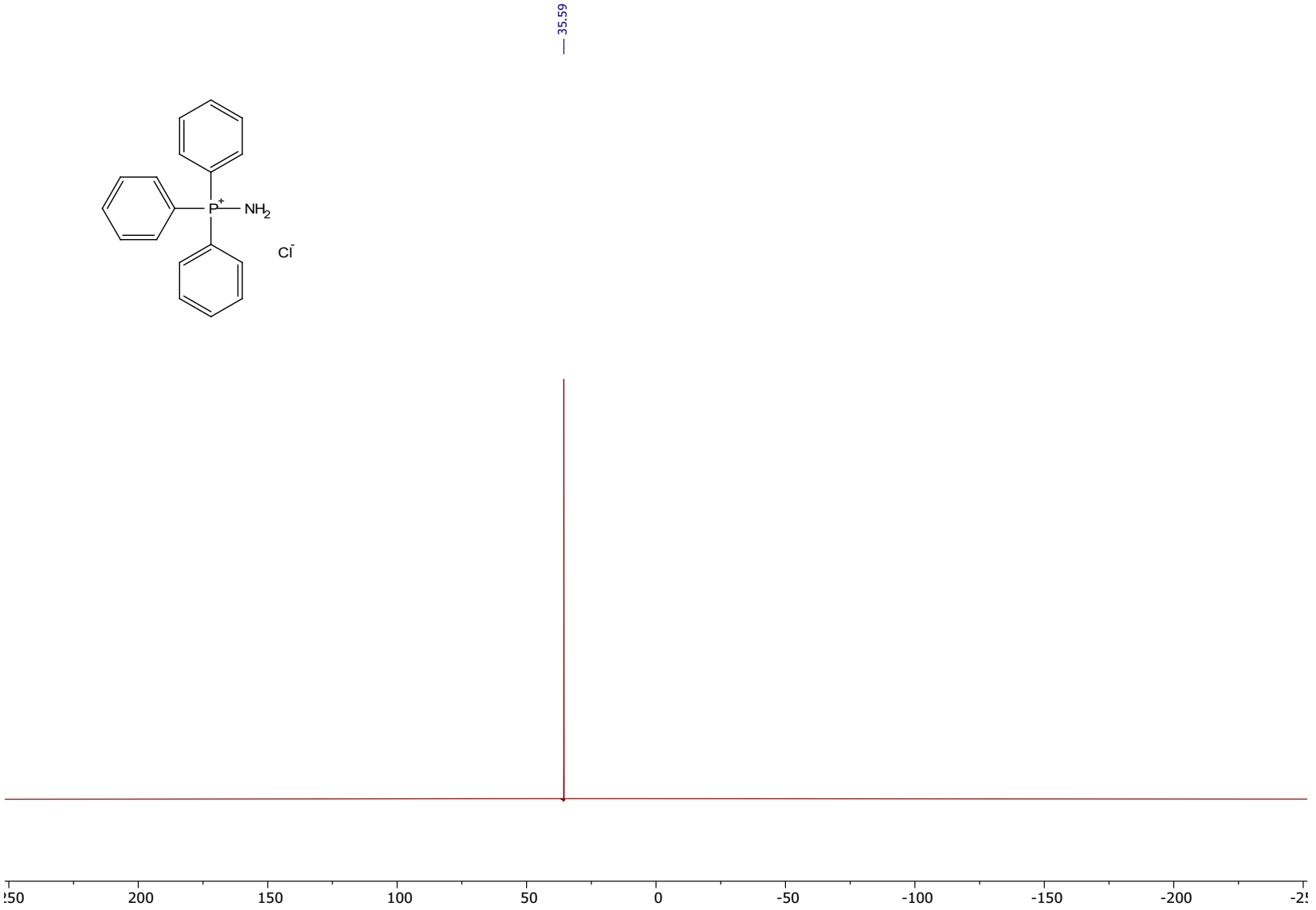

Figure S8. $^{31}P\{^{1}H\}$ NMR spectrum of aminotriphenylphosphonium chloride

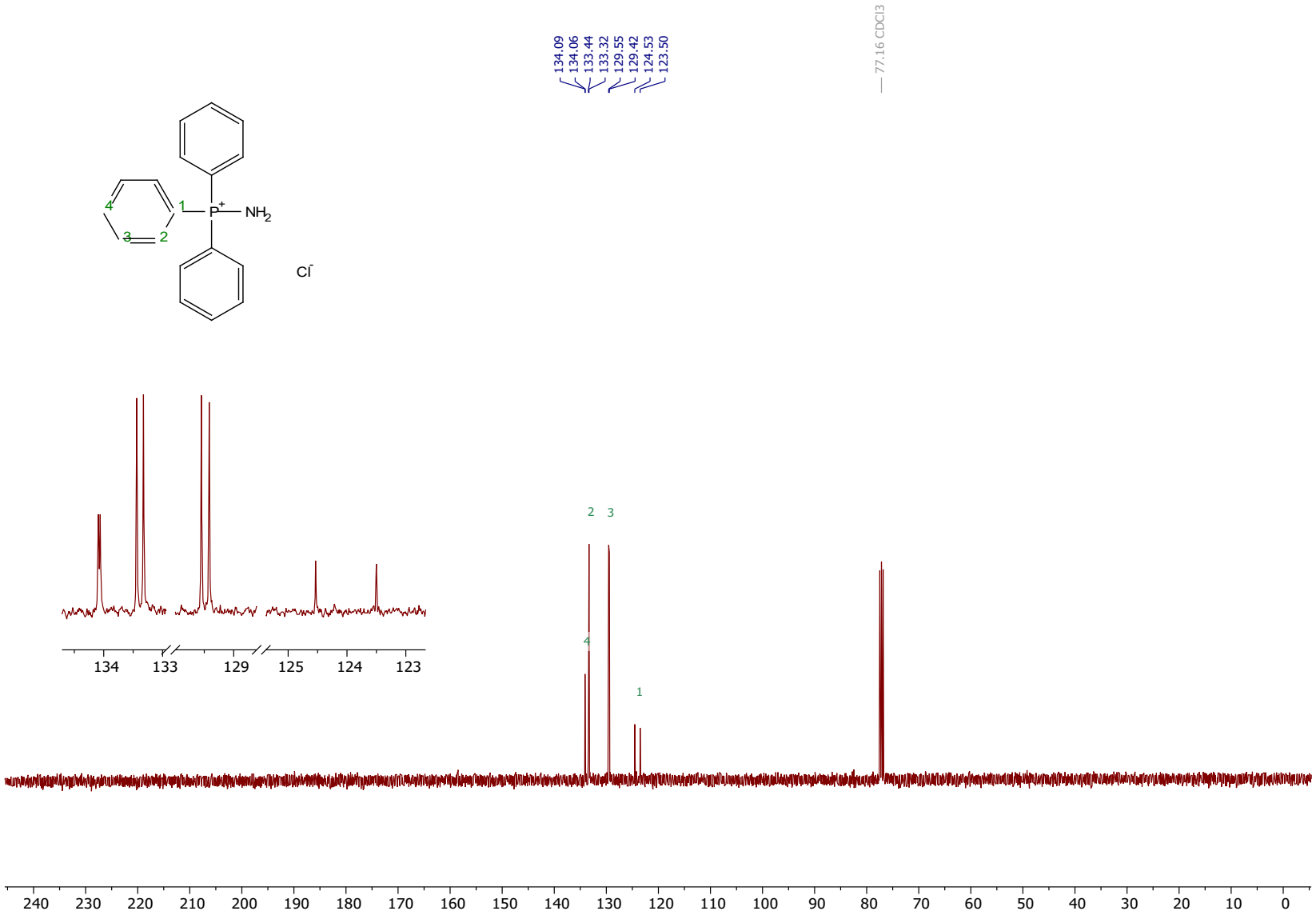

Figure S9. $^{13}C\{1H\}$ NMR spectrum of aminotriphenylphosphonium chloride

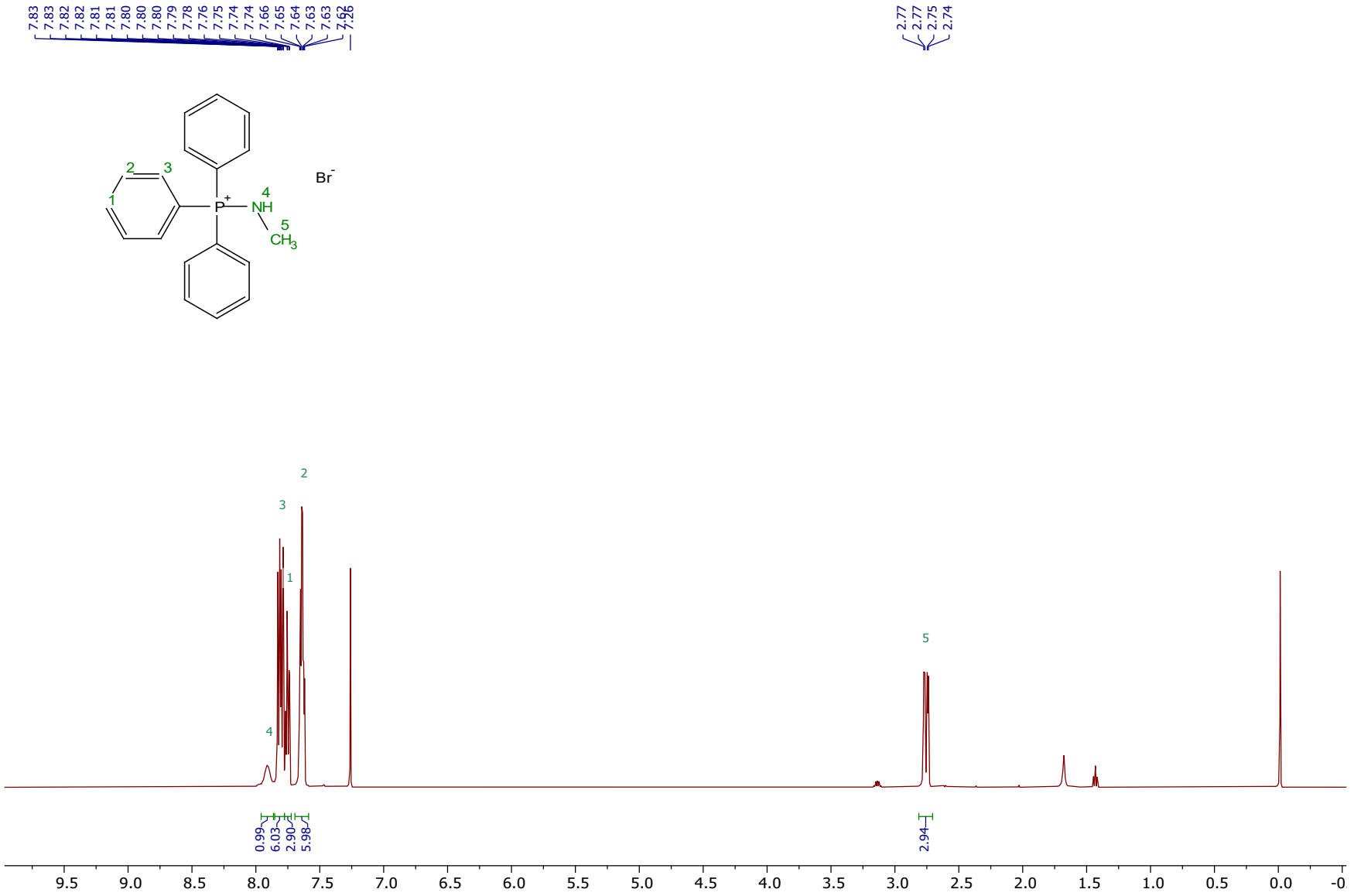

Figure S10. ^{1}H NMR spectrum of compound **2**

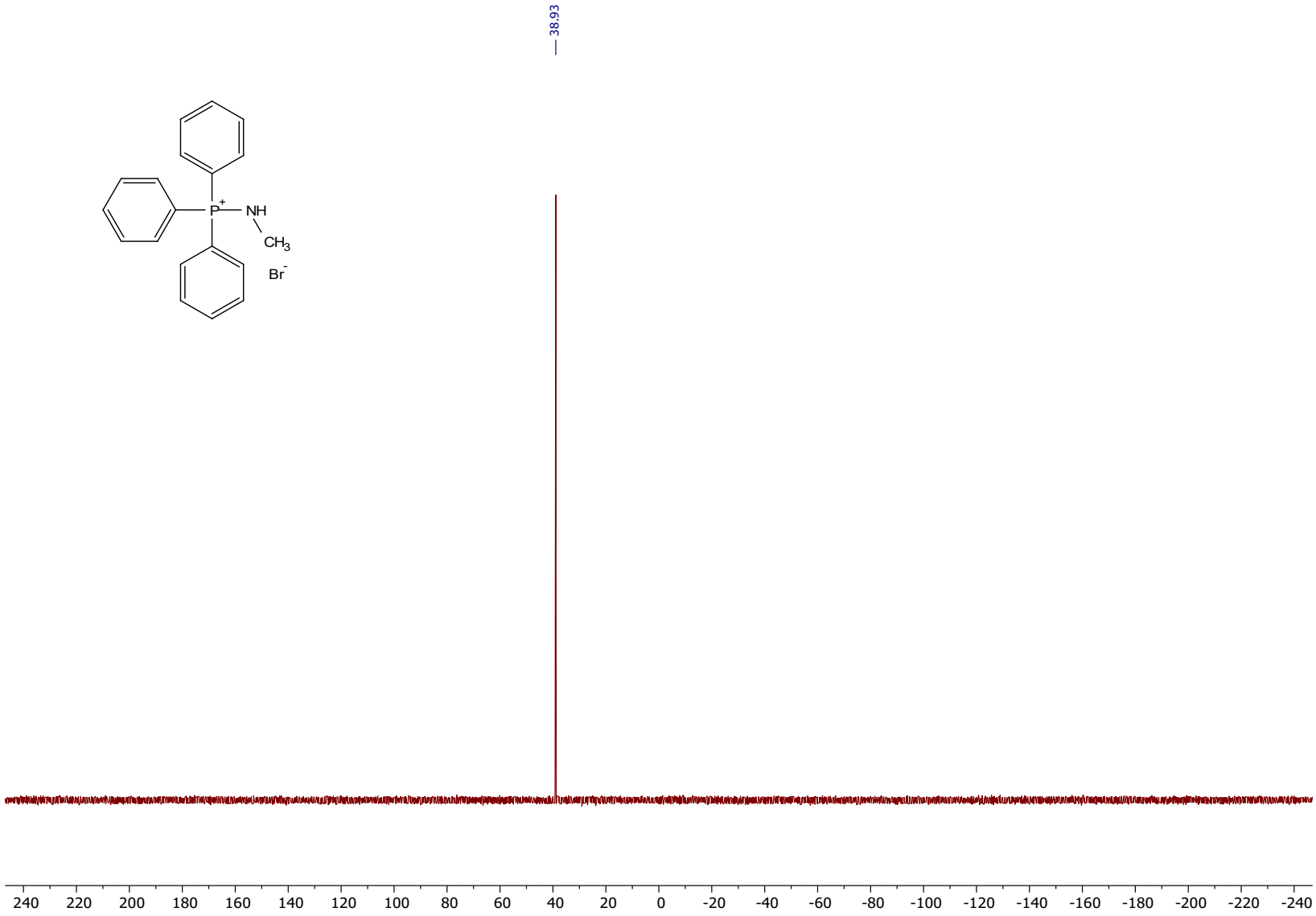

Figure S11. $^{31}P\{^{1}H\}$ NMR spectrum of compound **2**

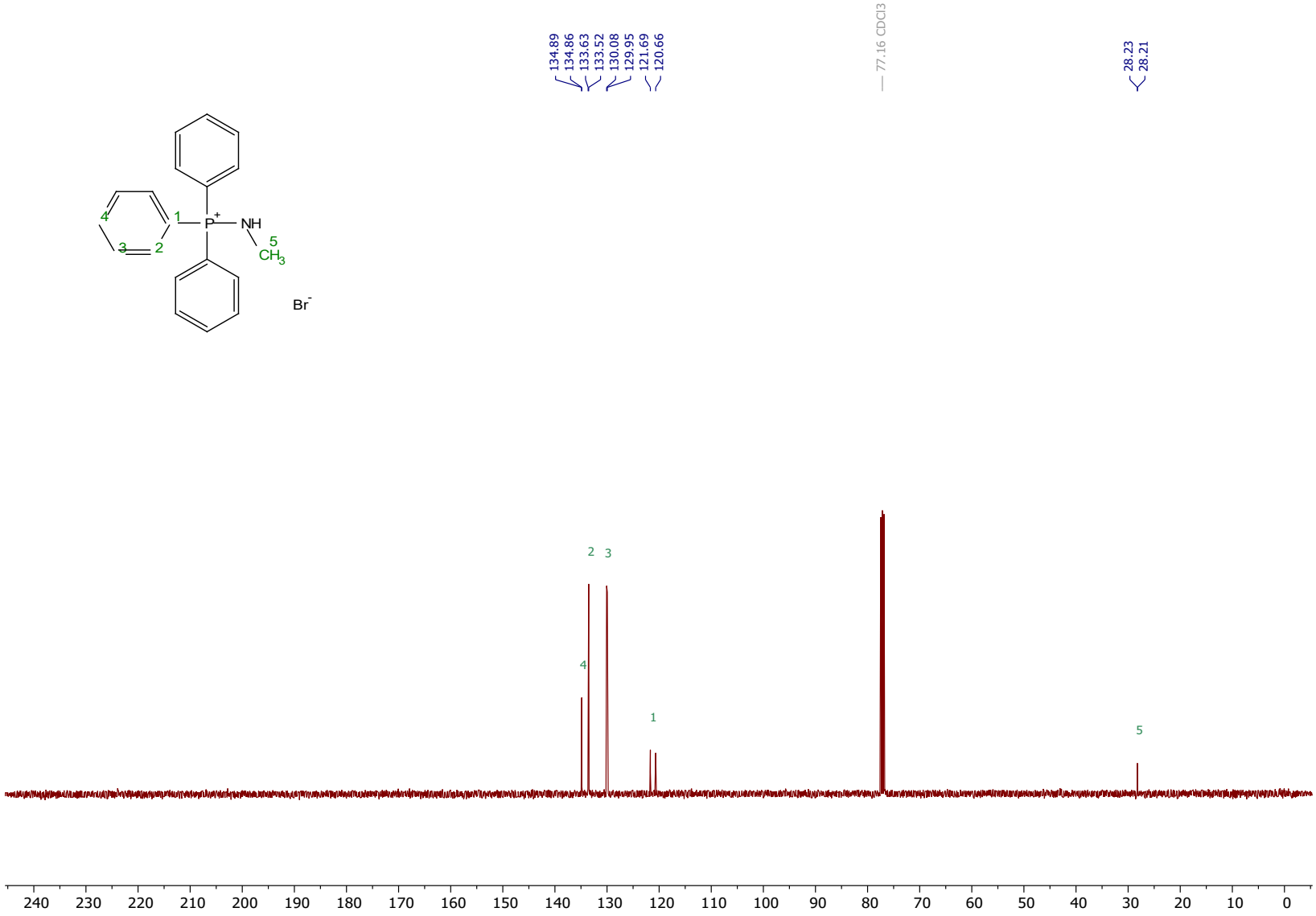

Figure S12. $^{13}C\{^{1}H\}$ NMR spectrum of compound **2**

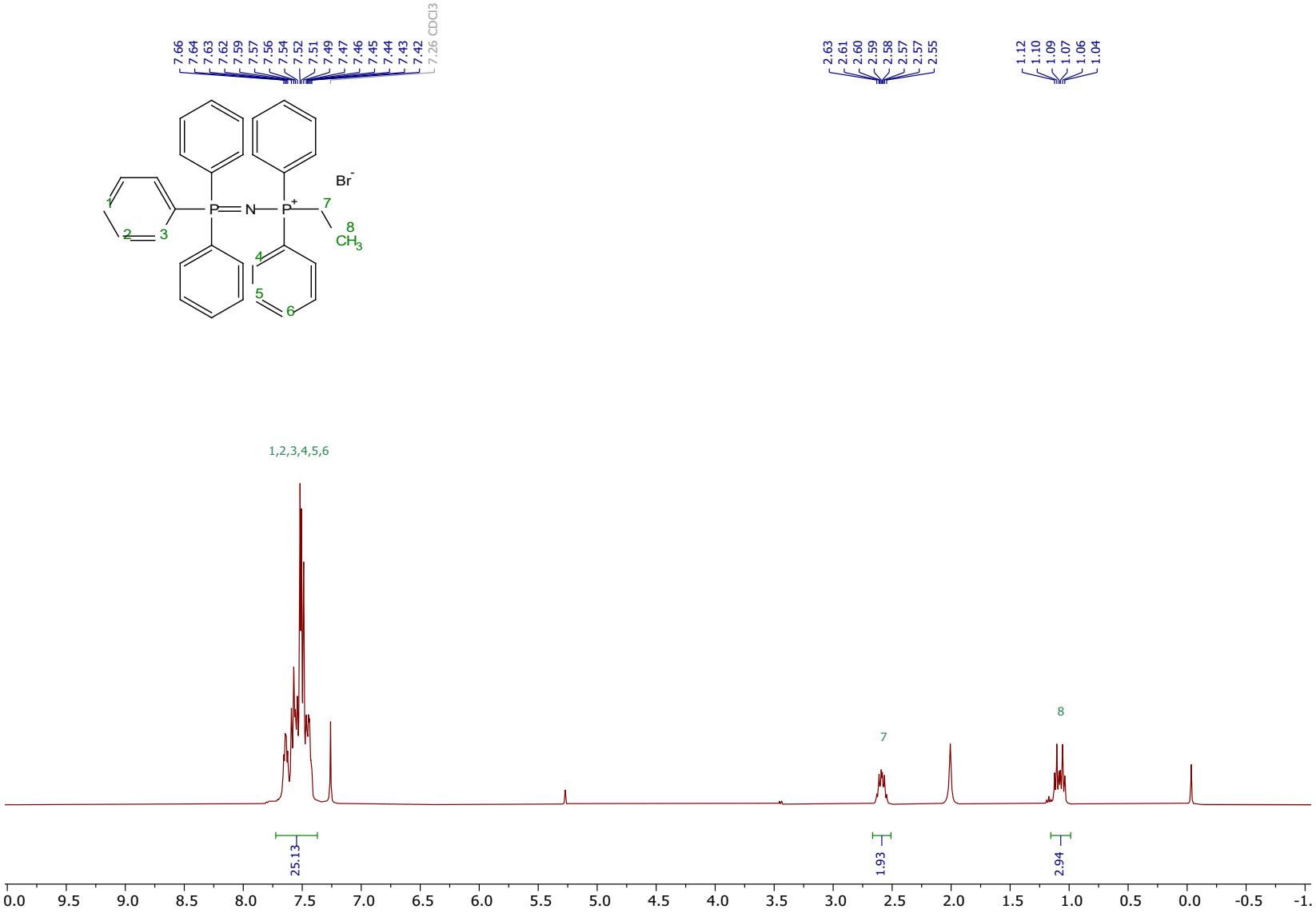

Figure S13. ^{1}H NMR spectrum of compound **3**

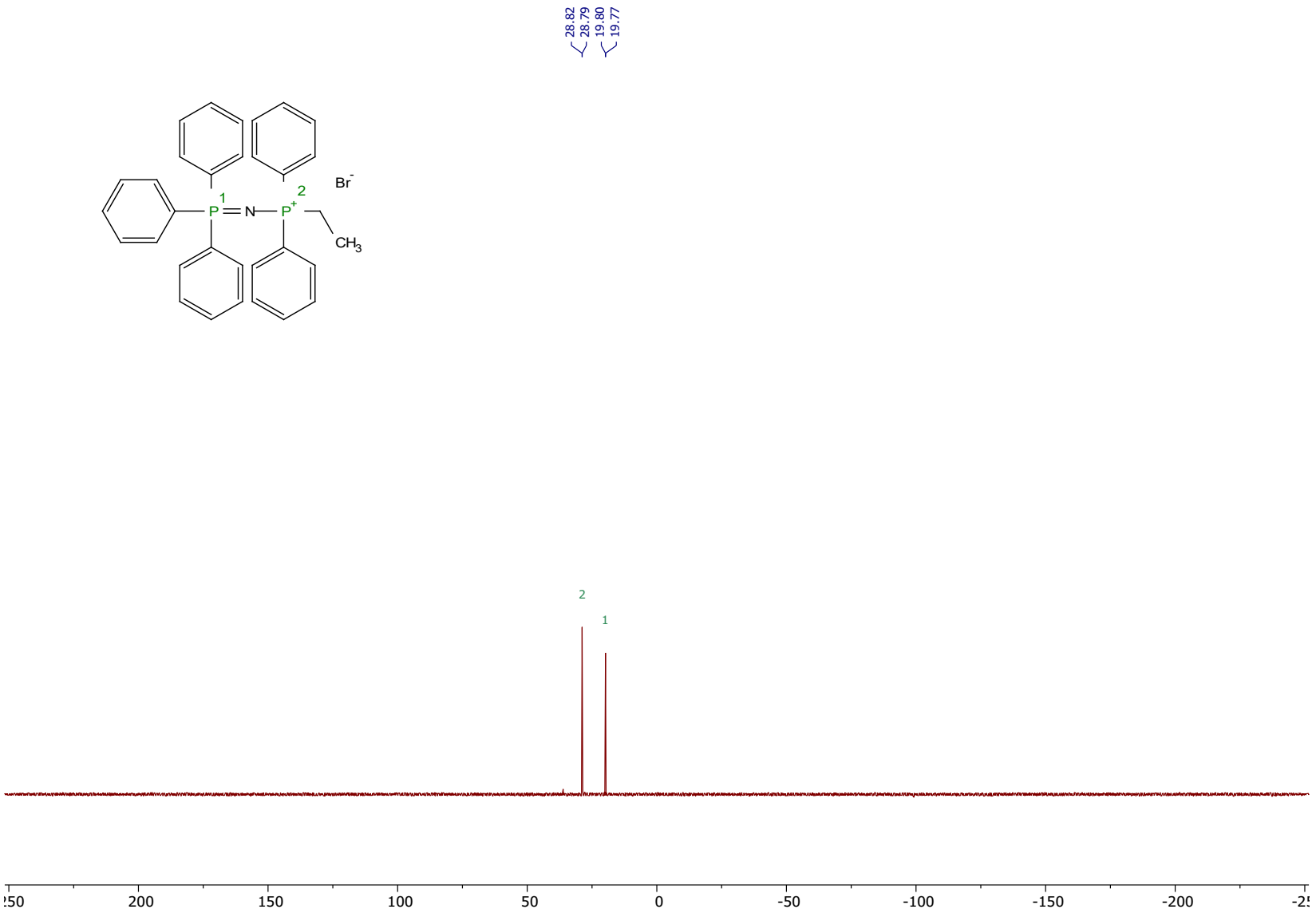

Figure S14. $^{31}P\{^{1}H\}$ NMR spectrum of compound **3**

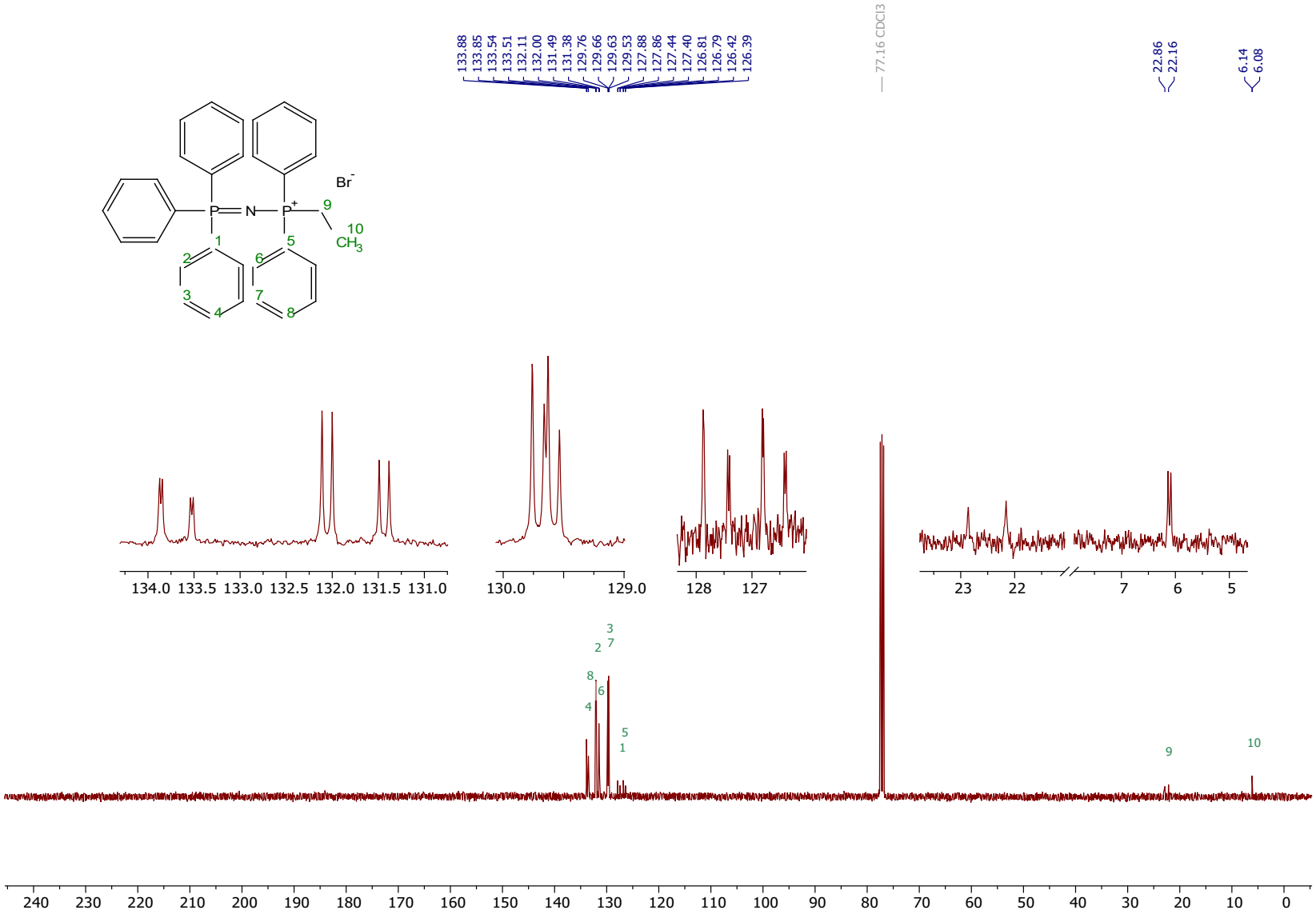

Figure S15. $^{13}C\{^{1}H\}$ NMR spectrum of compound **3**

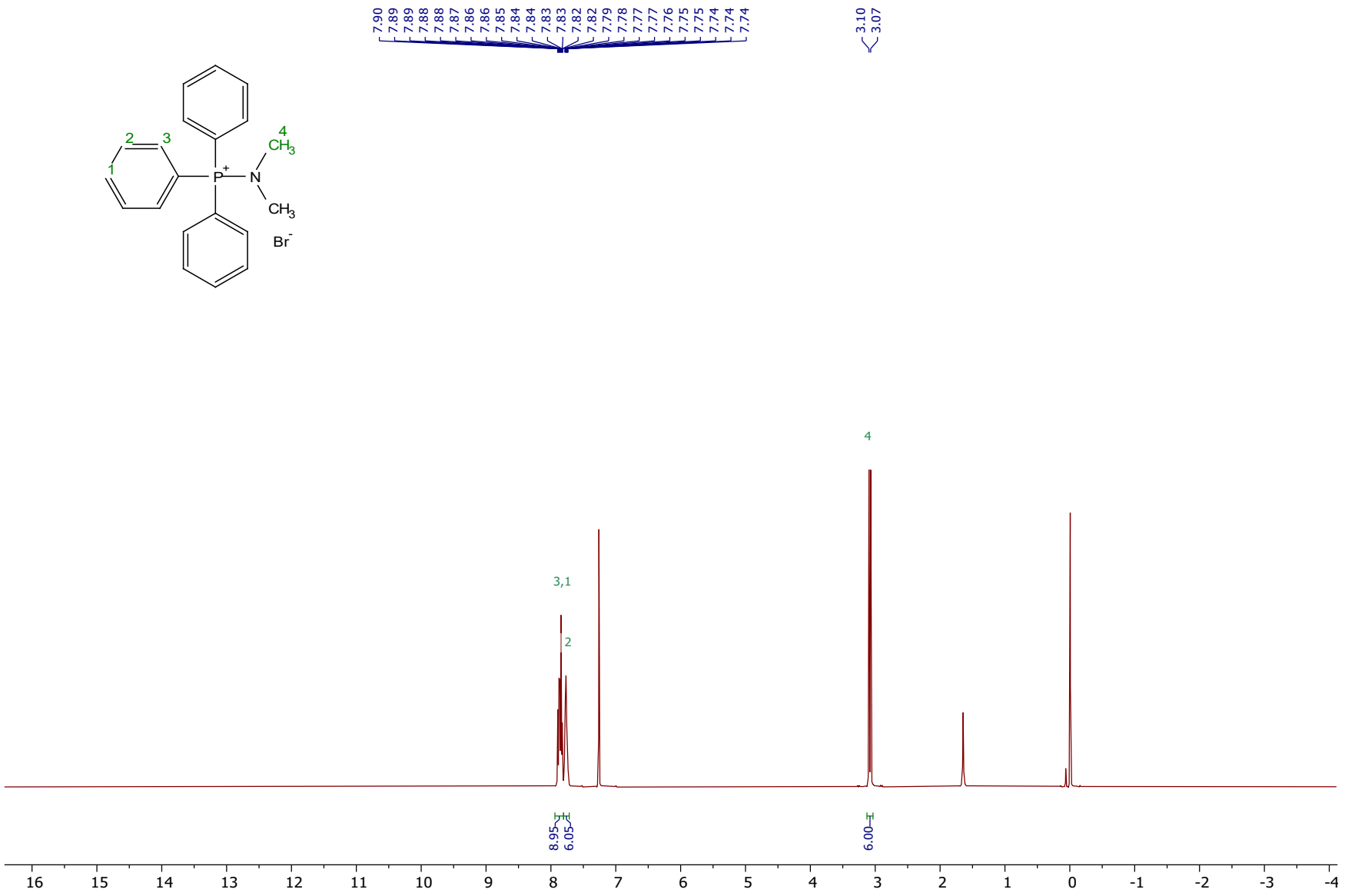

Figure S16. ^{1}H NMR spectrum of compound **4**

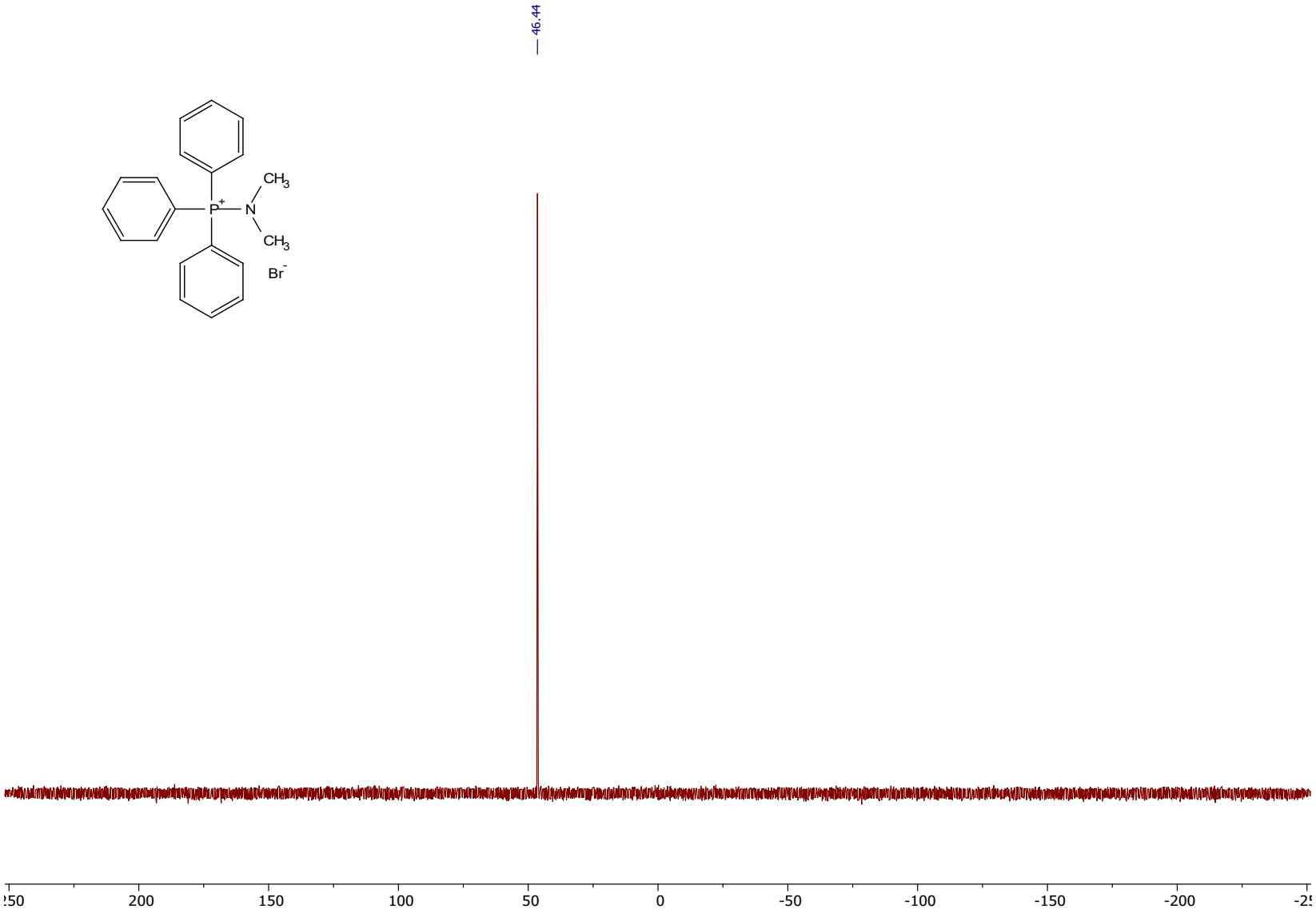

Figure S17. $^{31}P\{^{1}H\}$ NMR spectrum of compound **4**

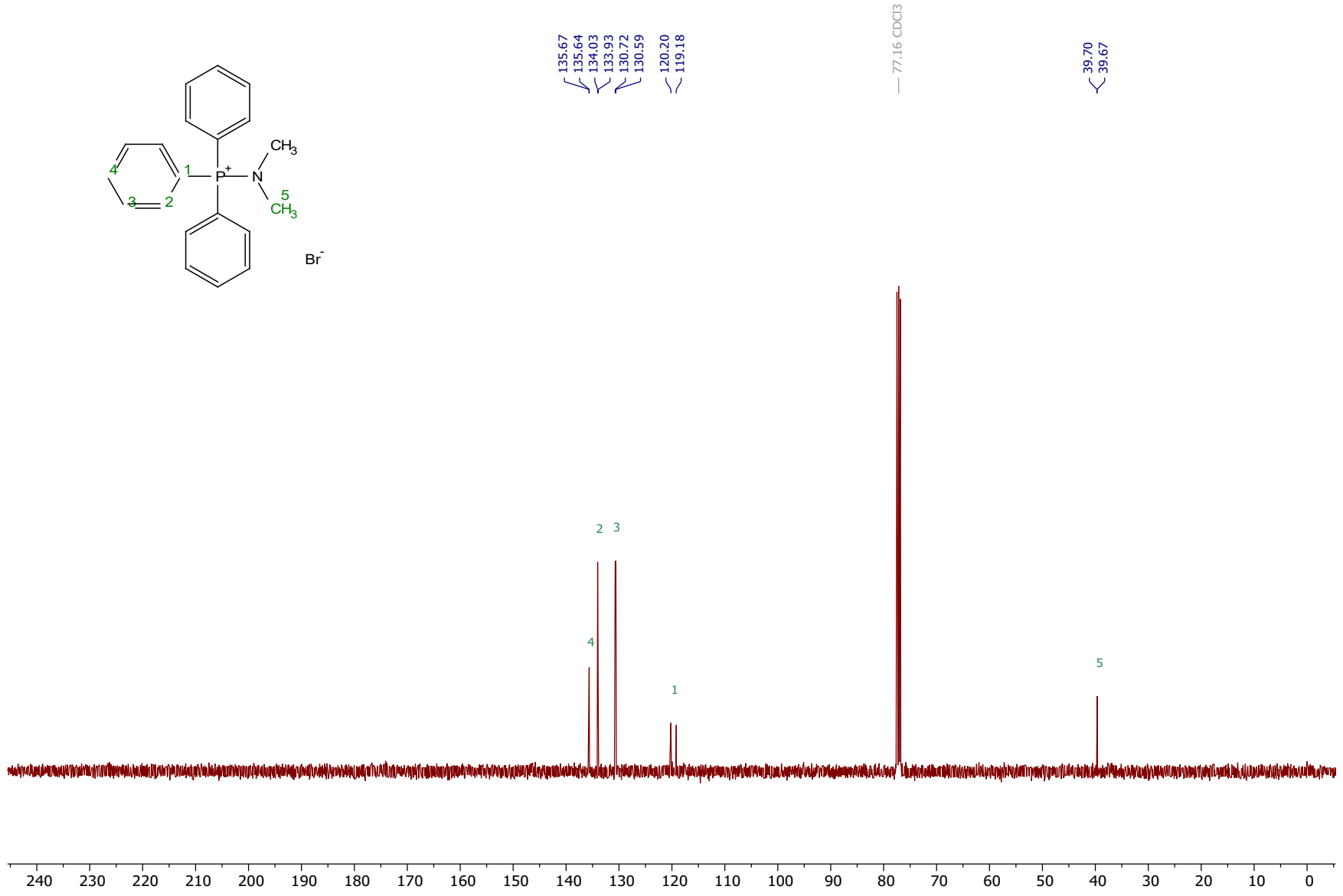

Figure S18. $^{13}C\{^{1}H\}$ NMR spectrum of compound **4**

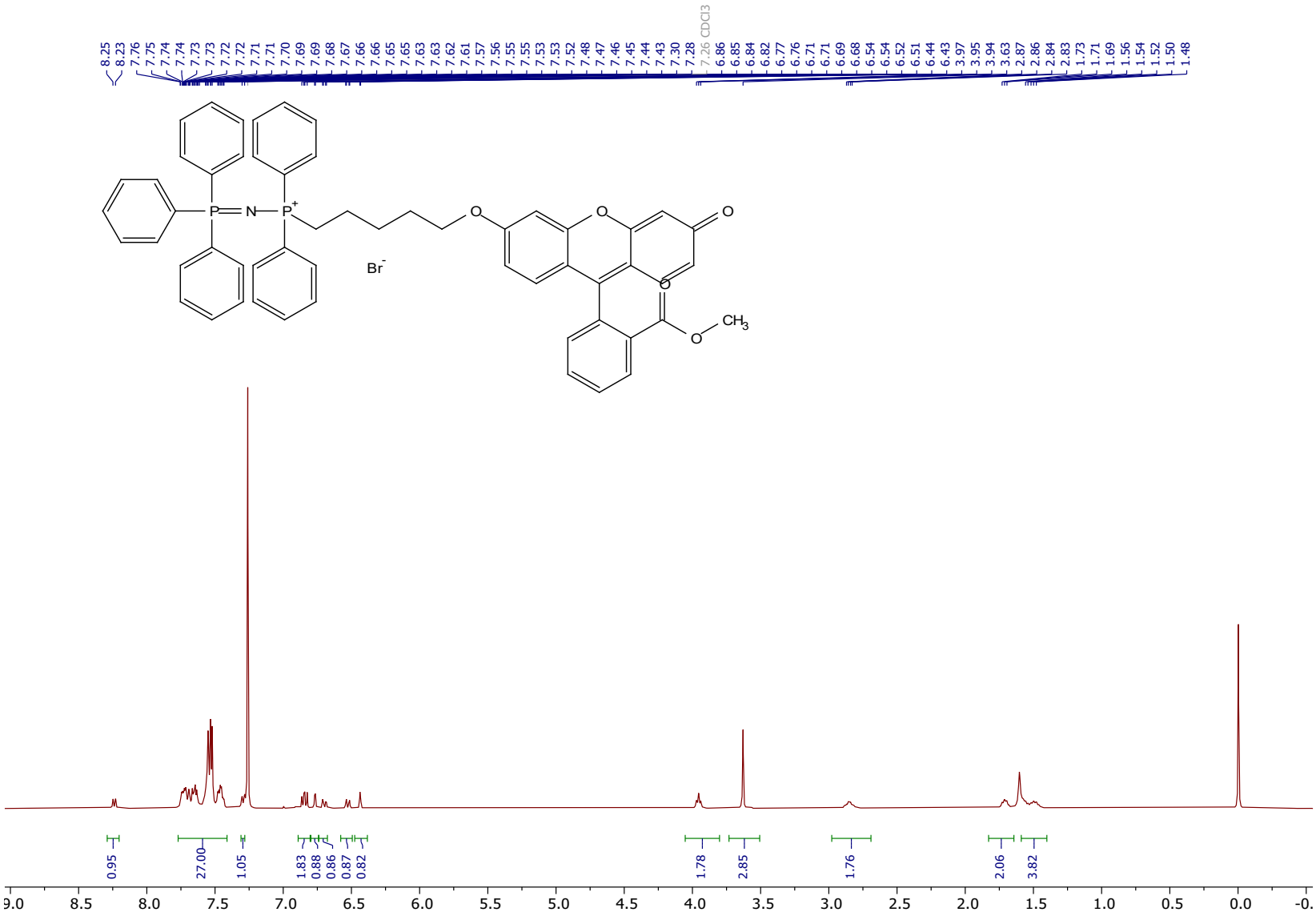

Figure S19. ^{1}H NMR spectrum of compound **7**

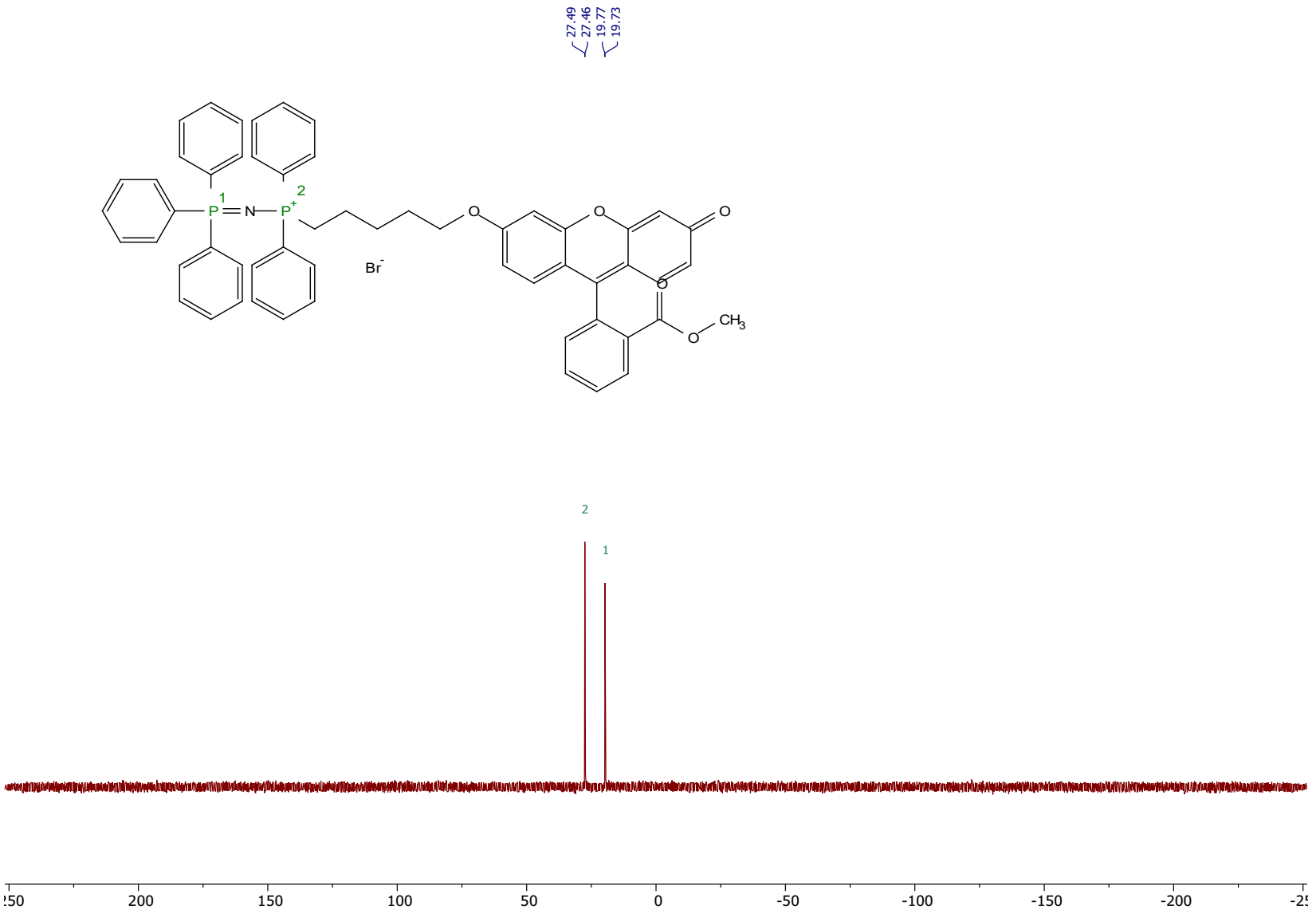

Figure S20. $^{31}P\{^{1}H\}$ NMR spectrum of compound **7**

10. High Resolution Mass Spectra

Elemental Composition Report

Tolerance = 10.0 PPM / DBE: min = -1.5, max = 50.0

Element prediction: Off

Number of isotope peaks used for i-FIT = 3

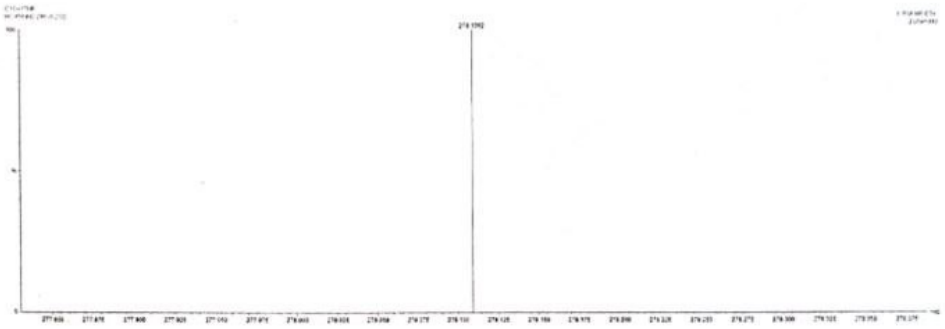

Monoisotopic Mass, Even Electron Ions

1 formula(e) evaluated with 1 results within limits (all results (up to 1000) for each mass)

Elements Used:

C: 18-18 H: 17-17 N: 1-1 P: 0-1

Minimum:			-1.5					
Maximum:	5.0	10.0	50.0					
Mass	Calc. Mass	mDa	PPM	DBE	i-FIT	Norm	Conf(%)	Formula
278.1092	278.1099	-0.7	-2.5	11.5	25.4	n/a	n/a	C18 H17 N P

Figure S21. High resolution mass spectrum for PPh_3-$NH_2^+Br^-$

Elemental Composition Report

Tolerance = 10.0 PPM / DBE: min = -1.5, max = 50.0

Element prediction: Off

Number of isotope peaks used for i-FIT = 3

Monoisotopic Mass, Even Electron Ions

7 formula(e) evaluated with 1 results within limits (up to 50 closest results for each mass)

Elements Used:

C: 15-25 H: 15-25 N: 0-1 P: 0-4

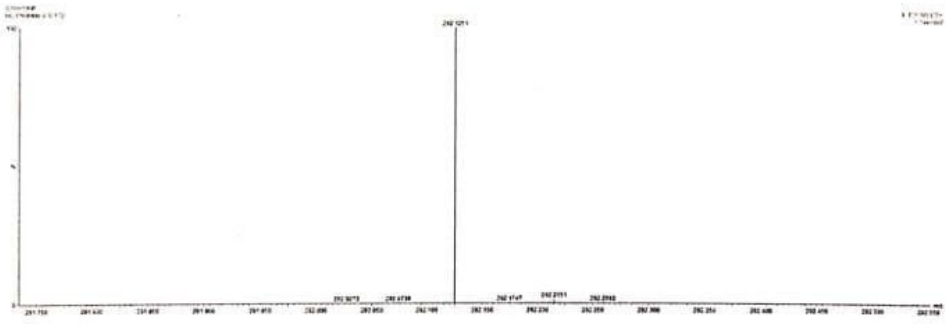

Minimum:	80.00			-1.5					
Maximum:	100.00	10.0	10.0	50.0					
Mass	RA	Calc. Mass	mDa	PPM	DBE	i-FIT	Norm	Conf(%)	Formula
292.1251	100.00	292.1255	-0.4	-1.4	11.5	104.9	n/a	n/a	C19 H19 N P

Figure S22. High resolution mass spectrum for compound **2**

Elemental Composition Report

Tolerance = 10.0 PPM / DBE: min = -1.5, max = 50.0

Element prediction: Off

Number of isotope peaks used for i-FIT = 3

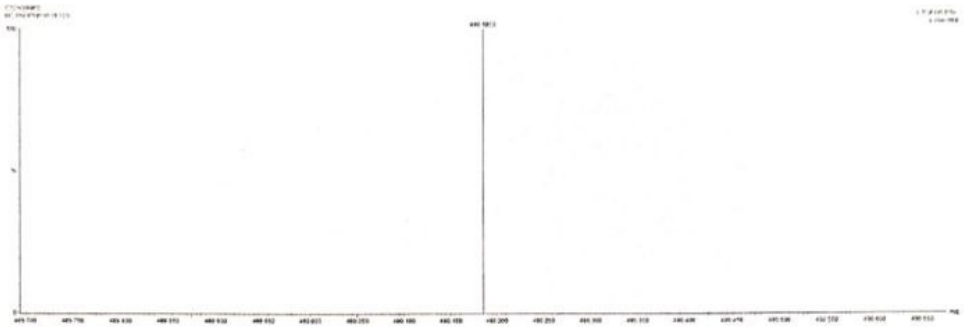

Monoisotopic Mass, Even Electron Ions

1 formula(e) evaluated with 1 results within limits (all results (up to 1000) for each mass)

Elements Used:

C: 32-32 H: 30-30 N: 1-1 P: 0-2

Minimum:			-1.5					
Maximum:	5.0	10.0	50.0					
Mass	Calc. Mass	mDa	PPM	DBE	i-FIT	Norm	Conf(%)	Formula
490.1853	490.1853	0.0	0.0	19.5	34.2	n/a	n/a	C32 H30 N P2

Figure S23. High resolution mass spectrum for compound **3**

Elemental Composition Report

Tolerance = 10.0 PPM / DBE: min = -1.5, max = 50.0

Element prediction: Off

Number of isotope peaks used for i-FIT = 3

Monoisotopic Mass, Even Electron Ions

4 formula(e) evaluated with 1 results within limits (up to 50 closest results for each mass)

Elements Used:

C: 20-20 H: 21-21 N: 1-1 P: 1-4

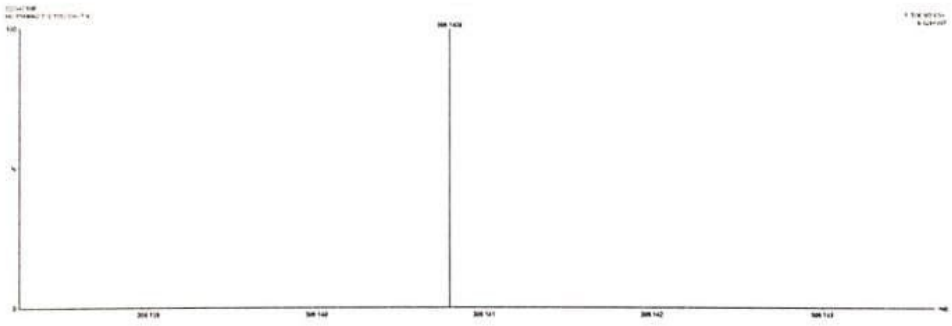

Minimum:	80.00			-1.5					
Maximum:	100.00	10.0	10.0	50.0					
Mass	RA	Calc. Mass	mDa	PPM	DBE	i-FIT	Norm	Conf(%)	Formula
306.1408	100.00	306.1412	-0.4	-1.3	11.5	1243.3		n/a n/a	C20 H21 N P

Figure S24. High resolution mass spectrum for compound **4**

Elemental Composition Report

Tolerance = 10.0 PPM / DBE: min = -1.5, max = 50.0

Element prediction: Off

Number of isotope peaks used for i-FIT = 3

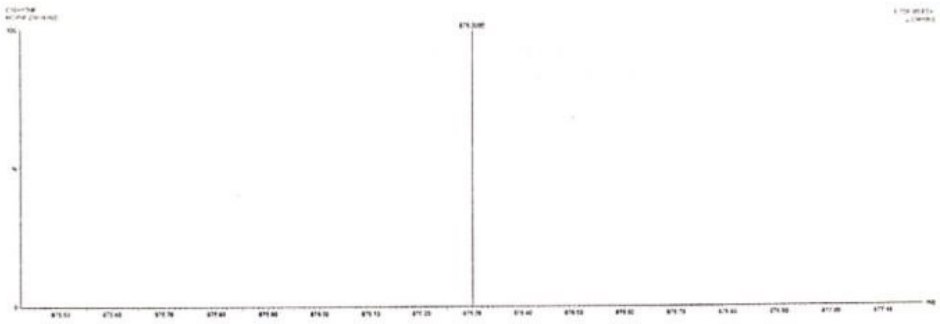

Monoisotopic Mass, Even Electron Ions

1 formula(e) evaluated with 1 results within limits (all results (up to 1000) for each mass)

Elements Used:

C: 56-56 H: 48-49 N: 1-1 O: 5-5 P: 0-2

Minimum:			-1.5					
Maximum:	5.0	10.0	50.0					
Mass	Calc. Mass	mDa	PPM	DBE	i-FIT	Norm	Conf(%)	Formula
876.3005	876.3008	-0.3	-0.3	34.5	27.1	n/a	n/a	C56 H48 N O5 P2

Figure S25. High resolution mass spectrum for **7**.

11. Single crystal X-ray data

Table S6. X-ray data of compounds **2 - 5**

	2	**3**	**4**	**5**
Empirical formula	$C_{19}H_{19}BrNP$	$C_{32}H_{30.50}BrNO_{0.25}P_2$	$C_{23}H_{29}BrNOP$	$C_{21}H22BrP$
Formula weight / g.mol^{-1}	455.39	574.92	446.35	385.26
Crystal system	triclinic	triclinic	orthorhombic	monoclinic
Space group	P -1	P -1	P b c a	P 1 21/n 1
a/ Å	9.4139(4)	10.3306(9)	13.9907(3)	10.6424(12)
b /Å	9.7021(4)	10.6126(9)	14.6428(4)	12.4166(15)
c/ Å	10.4201(4)	13.3397(11)	21.7567(6)	14.4706(17)
α/^{o}	63.4570(10)	82.341(3)	90	90
β/^{o}	80.694(2)	72.934(3)	90	93.167(4)
γ/^{o}	85.3810(10)	82.482(3)	90	90
Volume/ Å^3	840.16(6)	1379.1(2)	4457.1(2)	1909.3(4)
Z	2	2	8	4
ρ (Calc)/Mg.m^{-3}	1.471	1.384	1.330	1.340
Absorp. Coeff./ mm^{-1}	2.538	1.629	1.929	2.234
F(000)	380	593	1856	792
Crystal Size/ mm^3	0.060 x 0.120 x 0.220	0.160 x 0.200 x 0.220	0.125 x 0.200 x 0.250	0.300 x 0.300 x 0.400
Θ range/ ^{o}	2.19 to 39.50	2.24 to 35.80	2.22 to 30.52	2.32 to 26.37

Index range	-16<=h<=16 -17<=k<=17 18<=l<=18	-16<=h<=16 -17<=k<=16 -21<=l<=21	-19<=h<=19 -15<=k<=20 -31<=l<=31	-13<=h<=13 -15<=k<=12 -13<=l<=18
Refl. collected	32540	56112	45997	11725
Indep. Refns. (R_{int})	10017 (0.0794)	12774 (0.0917)	6800 (0.0864)	3901 (0.0666)
Completeness to Θ =	99.3%	99.2%	99.9%	99.9%
Absorp. Corr.	Multi-Scan	Multi-Scan	Multi-Scan	Multi-Scan
Max., min., transmission	0.8630 and 0.6050	0.7810 and 0.7160	0.7950 and 0.6440	0.5540 and 0.4680
Refinement Method	Full-matrix least-squares on F^2	Full-matrix least-squares on F^2	Full-matrix least-squares on F^2	Full-matrix least-squares on F^2
Data/ restraint/parameters	10017 / 1 / 204	12774 / 0 / 335	6800 / 0 / 249	3901 / 0 / 210
Goodness-of-fit on F^2	1.016	1.017	1.036	0.998
Final R indices [I>2σ(I)]	R1 = 0.0496 wR2 = 0.0857	R1 = 0.0528 wR2 = 0.1044	R1 = 0.0425 wR2 = 0.0821	R1 = 0.0504 wR2 = 0.0727
R indices (all data)	R1 = 0.1153 wR2 = 0.1048	R1 = 0.1151 wR2 = 0.1276	R1 = 0.0807 wR2 = 0.0954	R1 = 0.1175 wR2 = 0.0874
Largest diff. peak and hole/ e. $Å^{-3}$	0.621 and -0.988	0.609 and -0.742	0.516 and -0.567	0.340 and -0.481
Temperature/ K	100(2)	100(2)	100(2)	100(2)

References

1. SMART version 5.628; Bruker AXS Inc., Madison, WI, USA, 2001.
2. Sheldrick, G. M. SADABS V2014/4 (Bruker AXS Inc.) University of Göttingen, Göttingen, Germany, 2014.
3. SHELXL-2014/6 (Sheldrick, 2014); Bruker AXS Inc., Madison, WI, USA, 2014.
4. Hu, Z.; Sim, Y.; Kon, O. L.; Ng, W. H.; Ribeiro, A. J. M.; Ramos, M. J.; Fernandes, P. A.; Ganguly, R.; Xing, B. G.; Garcia, F.; Yeow, E. K. L., Unique Triphenylphosphonium Derivatives for Enhanced Mitochondrial Uptake and Photodynamic Therapy. Bioconjugate Chem 2017, 28 (2), 590-599.
5. Rezazgui, O.; Trouillas, P.; Qiu, S.-h.; Siegler, B.; Gierschner, J.; Leroy-Lhez, S., Synthesis and conformation of a novel fluorescein–Zn-porphyrin dyad and intramolecular energy transfer. New Journal of Chemistry 2016, 40 (4), 3843-3856.
6. Peters, M., Trobe, M., Tan, H., Kleineweischede, R. and Breinbauer, R., A Modular Synthesis of Teraryl-Based α-Helix Mimetics, Part 1: Synthesis of Core Fragments with Two Electronically Differentiated Leaving Groups. Chem. Eur. J., 2013, 19, 2442-2449.
7. H. C. Ong, J. T. S. Coimbra, G. Kwek, M. J. Ramos, B. Xing, P. A. Fernandes and F. García, RSC Chemical Biology, 2021, 2, 1643-1650.
8. Andres, A.; Roses, M.; Rafols, C.; Bosch, E.; Espinosa, S.; Segarra, V.; Huerta, J. M., Setup and validation of shake-flask procedures for the determination of partition coefficients (logD) from low drug amounts. Eur J Pharm Sci 2015, 76, 181-91.
9. Abraham, M. J.; Murtola, T.; Schulz, R.; Páll, S.; Smith, J. C.; Hess, B.; Lindahl, E., GROMACS: High performance molecular simulations through multi-level parallelism from laptops to supercomputers. SoftwareX 2015, 1-2, 19-25.
10. Berendsen, H. J. C.; Vanderspoel, D.; Vandrunen, R., Gromacs - a Message-Passing Parallel Molecular-Dynamics Implementation. Comput Phys Commun 1995, 91 (1-3), 43-56.
11. Van der Spoel, D.; Lindahl, E.; Hess, B.; Groenhof, G.; Mark, A. E.; Berendsen, H. J. C., GROMACS: Fast, flexible, and free. Journal of Computational Chemistry 2005, 26 (16), 1701-1718.
12. Jo, S.; Kim, T.; Iyer, V. G.; Im, W., CHARMM-GUI: a web-based graphical user interface for CHARMM. J Comput Chem 2008, 29 (11), 1859-65.
13. Qi, Y. F.; Ingolfsson, H. I.; Cheng, X.; Lee, J.; Marrink, S. J.; Im, W., CHARMM-GUI Martini Maker for Coarse-Grained Simulations with the Martini Force Field. J Chem Theory Comput 2015, 11 (9), 4486-4494.
14. Wu, E. L.; Cheng, X.; Jo, S.; Rui, H.; Song, K. C.; Davila-Contreras, E. M.; Qi, Y. F.; Lee, J. M.; Monje-Galvan, V.; Venable, R. M.; Klauda, J. B.; Im, W., CHARMM-GUI Membrane Builder Toward Realistic Biological Membrane Simulations. Journal of Computational Chemistry 2014, 35 (27), 1997-2004.
15. Lee, J.; Hitzenberger, M.; Rieger, M.; Kern, N. R.; Zacharias, M.; Im, W., CHARMM-GUI supports the Amber force fields. J Chem Phys 2020, 153 (3).
16. Wang, J. M.; Wang, W.; Kollman, P. A.; Case, D. A., Automatic atom type and bond type perception in molecular mechanical calculations. J Mol Graph Model 2006, 25 (2), 247-260.
17. Bayly, C. I.; Cieplak, P.; Cornell, W. D.; Kollman, P. A., A Well-Behaved Electrostatic Potential Based Method Using Charge Restraints for Deriving Atomic Charges - the Resp Model. J Phys Chem-Us 1993, 97 (40), 10269-10280.
18. Case D. A., B.-S. I. Y., Brozell S. R., Cerutti D. S., Cheatham, III T. E., Cruzeiro V. W. D., Darden T. A., Duke R. E., Ghoreishi D., Gilson M. K., Gohlke H., Goetz A. W., Greene D., Harris R., Homeyer N., Huang Y., Izadi S., Kovalenko A., Kurtzman T., Lee T. S., LeGrand S., Li P., Lin C., Liu J., Luchko T., Luo R., Mermelstein D. J., Merz K. M., Miao Y., Monard G., Nguyen C., Nguyen H., Omelyan I., Onufriev A., Pan F., Qi R., Roe D. R., Roitberg A., Sagui C., Schott-Verdugo S., Shen J., Simmerling C. L., Smith J., Salomon-Ferrer R., Swails J., Walker R. C., Wang J., Wei H., Wolf R. M., Wu X., Xiao L., York D. M., Kollman P. A., AMBER 2018. University of California, San Francisco 2018.

19. M. J. Frisch, G. W. T., H. B. Schlegel, G. E. Scuseria, M. A. Robb, J. R. Cheeseman, G. Scalmani, V. Barone, G. A. Petersson, H. Nakatsuji, X. Li, M. Caricato, A. Marenich, J. Bloino, B. G. Janesko, R. Gomperts, B. Mennucci, H. P. Hratchian, J. V. Ortiz, A. F. Izmaylov, J. L. Sonnenberg, D. Williams-Young, F. Ding, F. Lipparini, F. Egidi, J. Goings, B. Peng, A. Petrone, T. Henderson, D. Ranasinghe, V. G. Zakrzewski, J. Gao, N. Rega, G. Zheng, W. Liang, M. Hada, M. Ehara, K. Toyota, R. Fukuda, J. Hasegawa, M. Ishida, T. Nakajima, Y. Honda, O. Kitao, H. Nakai, T. Vreven, K. Throssell, J. A. Montgomery, Jr., J. E. Peralta, F. Ogliaro, M. Bearpark, J. J. Heyd, E. Brothers, K. N. Kudin, V. N. Staroverov, T. Keith, R. Kobayashi, J. Normand, K. Raghavachari, A. Rendell, J. C. Burant, S. S. Iyengar, J. Tomasi, M. Cossi, J. M. Millam, M. Klene, C. Adamo, R. Cammi, J. W. Ochterski, R. L. Martin, K. Morokuma, O. Farkas, J. B. Foresman, and D. J. Fox Gaussian 09, Revision D.01, Gaussian, Inc., Wallingford CT: 2016.

20. Hopkins, C. W.; Le Grand, S.; Walker, R. C.; Roitberg, A. E., Long-Time-Step Molecular Dynamics through Hydrogen Mass Repartitioning. J Chem Theory Comput 2015, 11 (4), 1864-1874.

21. Bussi, G.; Donadio, D.; Parrinello, M., Canonical sampling through velocity rescaling. J Chem Phys 2007, 126 (1).

22. MacCallum, J. L.; Bennett, W. F. D.; Tieleman, D. P., Distribution of amino acids in a lipid bilayer from computer simulations. Biophys J 2008, 94 (9), 3393-3404.

23. Marrink, S. J.; de Vries, A. H.; Mark, A. E., Coarse grained model for semiquantitative lipid simulations. J Phys Chem B 2004, 108 (2), 750-760.

24. Coimbra, J. T. S.; Feghali, R.; Ribeiro, R. P.; Ramos, M. J.; Fernandes, P. A., The importance of intramolecular hydrogen bonds on the translocation of the small drug piracetam through a lipid bilayer. Rsc Adv 2021, 11 (2), 899-9

25. MacCallum, J. L.; Tieleman, D. P., Computer simulation of the distribution of hexane in a lipid bilayer: Spatially resolved free energy, entropy, and enthalpy profiles. J Am Chem Soc 2006, 128 (1), 125-130.

26. Neale, C.; Bennett, W. F. D.; Tieleman, D. P.; Pomes, R., Statistical Convergence of Equilibrium Properties in Simulations of Molecular Solutes Embedded in Lipid Bilayers. J Chem Theory Comput 2011, 7 (12), 4175-41

27. Jambeck, J. P. M.; Lyubartsev, A. P., Implicit inclusion of atomic polarization in modeling of partitioning between water and lipid bilayers. Phys Chem Chem Phys 2013, 15 (13), 4677-468

28. Hub, J. S.; de Groot, B. L.; van der Spoel, D., g_wham-A Free Weighted Histogram Analysis Implementation Including Robust Error and Autocorrelation Estimates. J Chem Theory Comput 2010, 6 (12), 3713-3720.

29. Kumar, S.; Bouzida, D.; Swendsen, R. H.; Kollman, P. A.; Rosenberg, J. M., The Weighted Histogram Analysis Method for Free-Energy Calculations on Biomolecules .1. The Method. Journal of Computational Chemistry 1992, 13 (8), 1011-10

30. Humphrey, W.; Dalke, A.; Schulten, K., VMD: Visual molecular dynamics. J Mol Graph Model 1996, 14 (1), 33

31. Lu, T.; Chen, F., Multiwfn: A multifunctional wavefunction analyzer, J Comput Chem 2012, 33, 580-592

32. E. L. Robb, J. M. Gawel, D. Aksentijevic, H. M. Cocheme, T. S. Stewart, M. M. Shchepinova, H. Qiang, T. A. Prime, T. P. Bright, A. M. James, M. J. Shattock, H. M. Senn, R. C. Hartley and M. P. Murphy, Free Radical Biol. Med., 2015, 89, 883–894.